Title

The ion channel TRPV1 regulates the activation and proinflammatory properties of CD4+ T cells

Journal

Nature Immunology, 15(11)

ISSN

1529-2908

Authors

Bertin, Samuel
Aoki-Nonaka, Yukari
de Jong, Petrus Rudolf
et al.

Publication Date

2014-11-01

DOI

10.1038/ni.3009

Peer reviewed

HHS Public Access

Author manuscript

Nat Immunol. Author manuscript; available in PMC 2016 April 25.

Published in final edited form as:

Nat Immunol. 2014 November ; 15(11): 1055–1063. doi:10.1038/ni.3009.

The ion channel TRPV1 regulates the activation and proinflammatory properties of CD4+ T cells

Samuel Bertin[1], **Yukari Aoki-Nonaka**[1,2], **Petrus Rudolf de Jong**[1], **Lilian L. Nohara**[#3], **Hongjian Xu**[#3], **Shawna R. Stanwood**[3], **Sonal Srikanth**[4], **Jihyung Lee**[1], **Keith To**[1], **Lior Abramson**[1], **Timothy Yu**[1], **Tiffany Han**[1], **Ranim Touma**[5], **Xiangli Li**[1], **José M. González-Navajas**[1], **Scott Herdman**[1], **Maripat Corr**[1], **Guo Fu**[6,7], **Hui Dong**[1], **Yousang Gwack**[4], **Alessandra Franco**[5], **Wilfred A. Jefferies**[3,*], and **Eyal Raz**[1,*,¶]

[1]Department of Medicine, University of California, San Diego, La Jolla, CA 92093, USA.

[2]Division of Oral Science for Health Promotion, Niigata University Graduate School of Medical and Dental Sciences, 5274 Gakkocho 2-ban-cho, Chuo-ku, Niigata 951-8514, Japan.

[3]Michael Smith Laboratories; Centre for Blood Research; The Brain Research Centre; Department of Medical Genetics; Department of Microbiology and Immunology; Department of Zoology, University of British Columbia, Vancouver, BC, Canada.

[4]Department of Physiology, David Geffen School of Medicine at University of California, Los Angeles, Los Angeles, CA 90095, USA.

[5]Department of Pediatrics University of California, San Diego, La Jolla, CA 92093, USA.

[6]Department of Immunology and Microbial Science, IMM1, The Scripps Research Institute, 10550 North Torrey Pines Road, La Jolla, CA 92037, USA.

[7]State Key Laboratory of Cellular Stress Biology, Innovation Center for Cell Biology, School of Life Sciences, Xiamen University, Fujian 361102, China.

[#] These authors contributed equally to this work.

Abstract

TRPV1 is a Ca^{2+}-permeable channel mostly studied as a pain receptor in sensory neurons. However, its role in other cell types is poorly understood. Here, we demonstrate that TRPV1 is functionally expressed in $CD4^+$ T cells where it acts as a non-store-operated Ca^{2+} channel and

[¶]Corresponding author: Eyal Raz M.D, eraz@ucsd.edu.
[*]Senior authors.

AUTHOR CONTRIBUTIONS

S.B., P.R.d.J., A.F. and E.R. designed the study; S.B., Y.A.-N., P.R.d.J., K.T., L.A., T.Y., T.H., X.L. and J.M.G.-N. performed most of the *in vitro* and *in vivo* experiments; S.B. measured the Ca^{2+} flux by flow cytometry, with the technical assistance of X.L. and G.F.; S.S. and Y.G. performed single-cell Ca^{2+} imaging in mouse $CD4^+$ T cells; S.B. and J.L., with the help of H.D., performed single-cell Ca^{2+} imaging in Jurkat cells; L.L.N., H.X., S.R.S. and W.A.J. planned and designed the electrophysiological assays, L.L.N., H.X. and S.R.S. performed these assays, and L.L.N., H.X., S.R.S., and W.A.J. wrote the corresponding sections of the manuscript; R.T. and A.F. performed the human T cell experiments with TRPV1 antagonists; S.H. and M.C. took care of the mouse colony and genotyped the mice; S.B., Y.A.-N., P.R.d.J., T.Y., K.T., L.A., A.F. and E.R. analyzed and interpreted the data; and S.B. and E.R. wrote the manuscript.

COMPETING FINANCIAL INTERESTS

The authors declare no competing financial interests.

contributes to T cell receptor (TCR)-induced Ca^{2+} influx, TCR signaling and T cell activation. In models of T cell-mediated colitis, TRPV1 promotes colitogenic T cell responses and intestinal inflammation. Furthermore, genetic and pharmacological inhibition of TRPV1 in human $CD4^+$ T cells recapitulates the phenotype of murine *Trpv1*$^{-/-}$ $CD4^+$ T cells. These findings suggest that TRPV1 inhibition could represent a new therapeutic strategy to restrain proinflammatory T cell responses.

Following engagement of the T cell receptor (TCR) and formation of the immunological synapse, calcium (Ca^{2+}) channels mediate the Ca^{2+} influx necessary for the activation of T cells[1]. Ca^{2+} influx from the extracellular milieu into the cytosol is mandatory for the activation of downstream TCR signaling pathways and key transcription factors, including NFAT and NF-κB[2]. TCR ligation triggers phosphorylation events that lead to the activation of the Ca^{2+} release-activated Ca^{2+} (CRAC) channel complex and to store-operated Ca^{2+} entry (SOCE)[3]. However, this canonical scheme of Ca^{2+} influx does not account for the involvement of other plasma-membrane Ca^{2+} channels.

Studies have documented the important contribution of voltage-gated Ca^{2+} channels (Ca_V)[4,5] and members of the Transient Receptor Potential (TRP) family of ion channels[6,7] to T cell activation. The mammalian TRP family of ion channels consists of 28 members divided into six subfamilies: 7 TRPC (Canonical), 6 TRPV (Vanilloid), 8 TRPM (Melastatin), 1 TRPA (Ankyrin), 3 TRPP (Polycystin) and 2 TRPML (Mucolipin)[8]. Although physiological roles of TRP channels are well characterized in the nervous system, their role in T cell activation and function is still elusive[2, 5, 6].

The founding member of the TRPV subfamily, TRPV1, is highly permeable to Ca^{2+} ($P_{Ca}/P_{Na} \approx 10$)[9] and was initially identified as the receptor for capsaicin, the pungent ingredient in chili peppers[10]. In this study, we report that mouse and human primary $CD4^+$ T cells express a functional TRPV1 channel (termed here as 'TRPV1^{CD4}'). We identified that TRPV1^{CD4} contributes to TCR-induced Ca^{2+} influx and is required for proper downstream TCR signaling. Our data indicate a cell-intrinsic role for the TRPV1 channel in the activation and the acquisition of proinflammatory properties by $CD4^+$ T cells.

RESULTS

TRPV1 channel is expressed and functional in $CD4^+$ T cells

We first compared the mRNA expression levels of various TRP channels in primary $CD4^+TCR\beta^+$ T cells isolated from the spleens (SP) of C57BL/6 (WT) mice. Among the 8 different TRP channels analyzed, *Trpv1* transcript level was the highest **(Fig. 1a)**. $CD4^+$ T cells isolated from *Trpv1*$^{-/-}$ mice were used as control **(Fig. 1b)**. We confirmed TRPV1 protein expression in murine SP $CD4^+$ T cells, in human primary $CD4^+$ T cells and in the human Jurkat T cell line by immunoblotting **(Supplementary Fig. 1a)** and by flow cytometry **(Fig. 1c)**. We identified by confocal microscopy **(Fig. 1d** and **Supplementary Fig. 1b,c)** that TRPV1 is predominantly expressed at the plasma membrane of resting $CD4^+$ T cells. Indeed, the fluorescence signals of TRPV1 and CD4 were largely colocalized (Pearson's Correlation coefficient [Rr] = 0.96) **(Fig. 1e)**. Furthermore, cell-surface

biotinylation assays confirmed TRPV1 localization at the plasma membrane of Jurkat T cells **(Supplementary Fig. 1d)**

We next evaluated TRPV1 channel functionality in $CD4^+$ T cells by employing the whole-cell patch clamp technique. We used the prototypical TRPV1 agonist capsaicin (CAP)[10] and recorded CAP-evoked currents in WT and *Trpv1*$^{-/-}$ $CD4^+$ T cells held at −85 mV **(Fig. 2a)**. In WT $CD4^+$ T cells, CAP application rapidly induces a small inward current (1.7 ± 0.4 pA/pF, n = 9) that was desensitized with prolonged agonist exposure **(Fig. 2a,b)**. This desensitization was likely caused by the presence of Ca^{2+} ions in the external solution as previously demonstrated in recording rat (r)TRPV1 current in HEK293 cells[10, 11]. In *Trpv1*$^{-/-}$ $CD4^+$ T cells, only an insignificant amount of inward current (0.4 ± 0.1 pA/pF, n = 8) was recorded in response to CAP. Additionally, using the same recording conditions, we routinely recorded 2-10 nA CAP-gated currents from transformed human kidney (tSA201) cells transiently expressing rTRPV1 (data not shown). To further confirm that the current observed in WT $CD4^+$ T cells was indeed a TRPV1 current, we measured CAP-induced currents in the presence of SB366791 (SB), a specific TRPV1 antagonist[12]. SB inhibited approximately 80% of the inward current observed in WT $CD4^+$ T cells in response to CAP (control 2.0 ± 0.3 pA/pF, n = 10 and SB-treated 0.4 ± 0.1 pA/pF, n = 13) **(Fig. 2a,c)**. To better characterize the CAP-induced current in $CD4^+$ T cells we used a ramp pulse protocol to measure current-voltage relationship (I-V curve) upon addition of CAP **(Fig. 2d)**. The I-V relationship of CAP-gated current confirms the outward rectification characteristic of TRPV1 current previously reported for the rat and the human TRPV1 channels[10,12].

To further evaluate TRPV1 channel functionality in $CD4^+$ T cells we performed single-cell ratiometric Ca^{2+} imaging and flow cytometry-based Ca^{2+} flux measurements. CAP concentration-dependently increased the intracellular calcium concentration ($[Ca^{2+}]_i$) in WT but not in *Trpv1*$^{-/-}$ naive $CD4^+$ T cells **(Fig. 2e,f)**. In addition, we generated CD4-specific TRPV1 transgenic (*Trpv1*^{Tg}) mice by crossing *Rosa26-Trpv1* mice[13] with *Cd4*-Cre mice and found that CAP induced a dramatic Ca^{2+} influx in *Trpv1*^{Tg} $CD4^+$ T cells **(Fig. 2e,f)** that overexpress TRPV1 **(Fig. 2g)**. CAP also induced a significant Ca^{2+} influx in Jurkat T cells, which was almost completely abolished after shRNA-mediated knockdown of TRPV1 **(Supplementary Fig. 1e)**. Collectively, these findings indicate that the TRPV1 channel is functionally expressed on the plasma membrane of $CD4^+$ T cells (hereafter termed $TRPV1^{CD4}$).

$TRPV1^{CD4}$ contributes to TCR-induced Ca^{2+} influx

We next investigated the physiological role of $TRPV1^{CD4}$ by comparing changes in $[Ca^{2+}]_i$ after TCR stimulation in WT, *Trpv1*$^{-/-}$ and *Trpv1*^{Tg} $CD4^+$ T cells. Ca^{2+} influx induced by anti-CD3 antibody crosslinking was significantly reduced in *Trpv1*$^{-/-}$ $CD4^+$ T cells compared to WT cells **(Fig. 3a,b)**. This defect in *Trpv1*$^{-/-}$ $CD4^+$ T cells was observed independently of the extracellular calcium concentration ($[Ca^{2+}]_e$) tested and of the Ca^{2+} flux monitoring protocol used (e.g., TCR stimulation prior to $CaCl_2$ addition or vice versa) **(Supplementary Fig. 2a-d)**. In addition, Ca^{2+} titration experiments revealed that the TCR-induced Ca^{2+} influx defect in *Trpv1*$^{-/-}$ $CD4^+$ T cells could be rescued by a 50% increase in $[Ca^{2+}]_e$ in the culture medium **(Fig. 3c)**. In accordance with the localization of $TRPV1^{CD4}$ at

the plasma membrane **(Fig. 1d,e** and **Supplementary Fig. 1d)**, the Ca^{2+} efflux from intracellular stores was similar in WT and *Trpv1*$^{-/-}$ $CD4^+$ T cells after TCR stimulation **(Supplementary Fig. 2e)**. The TCR-induced Ca^{2+} influx was significantly more sustained in *Trpv1*^{Tg} $CD4^+$ T cells compared to WT cells **(Fig. 3a,b** and **Supplementary Fig. 2f)**. However, no differences in Ca^{2+} influx were observed between WT, *Trpv1*$^{-/-}$ and *Trpv1*^{Tg} $CD4^+$ T cells following stimulation with the Ca^{2+} ionophore, ionomycin **(Fig. 3a,b** and **Supplementary Fig. 2g,h)** or with the sarcoplasmic reticulum Ca^{2+}-ATPase (SERCA) pump inhibitor, thapsigargin **(Fig. 3d,e** and **Supplementary Fig. 2i)** that bypass proximal TCR signaling and induce CRAC channel activation and SOCE[14]. Since TRPV3 shares 40-50% homology and can form heteromultimers with TRPV1[9,15], we also analyzed the Ca^{2+} influx profile of SP $CD4^+$ T cells isolated from *Trpv3*$^{-/-}$ mice. However, in contrast to *Trpv1*$^{-/-}$ $CD4^+$ T cells, we found normal Ca^{2+} influx in these cells upon TCR stimulation **(Supplementary Fig. 2j)**. We further confirmed the specific contribution of TRPV1 to TCR-induced Ca^{2+} currents by performing whole-cell patch clamp experiments. TCR-crosslinking produced significantly smaller inward currents in *Trpv1*$^{-/-}$ $CD4^+$ T cells (4.1 ± 0.6 pA/pF, n = 9) held at −85 mV, compared to WT cells (12.3 ± 3.3 pA/pF, n = 7) under the same experimental conditions **(Fig. 2f,g)**. Finally, the pre-treatment of WT $CD4^+$ T cells with two different TRPV1 antagonists, BCTC[16] **(Fig. 3h,i)** or I-RTX[17] **(Supplementary Fig. 2k)**, concentration-dependently decreased the Ca^{2+} influx induced by TCR stimulation to a level comparable to *Trpv1*$^{-/-}$ $CD4^+$ T cells. Collectively, these results suggest that $TRPV1^{CD4}$ acts as a non-store-operated Ca^{2+} channel and contributes to TCR-induced Ca^{2+} influx.

$TRPV1^{CD4}$ is part of the TCR signaling cascade

We then investigated how $TRPV1^{CD4}$ is activated upon TCR stimulation and assessed its impact on TCR signaling. We first compared TRPV1 subcellular localization in resting and activated $CD4^+$ T cells by confocal microscopy. We found that TRPV1 colocalizes with components of the TCR complex such as CD4 **(Fig. 1d,e)** and Lck **(Fig. 4a)** under resting conditions. In addition, Lck and TRPV1 are rapidly recruited to TCR clusters after TCR ligation. Since the formation of the cap structure is known to be dependent on tyrosine phosphorylation[18, 19], we analyzed whether TRPV1 clustering is dependent on a similar mechanism. Indeed, the Src-family kinase inhibitor PP2[20] inhibited Lck and TRPV1 capping **(Fig. 4a)**.

Because phosphorylation of TRP channels regulates their channel activity[21-23], we investigated whether TCR engagement induces $TRPV1^{CD4}$ tyrosine phosphorylation. To address the possible role of Lck in this system, we examined the tyrosine phosphorylation status of endogenous TRPV1 immunoprecipitated from Jurkat T cells (clone E6.1) and a derivative mutant (J.CaM1.6), which lack Lck expression[24]. TCR stimulation induced TRPV1 tyrosine phosphorylation in the parental cell line (WT) but not in the Lck-deficient mutant (*Lck*$^{-/-}$) **(Fig. 4b)**. In accordance with previous studies that have demonstrated the essential role of Src-family kinases in TRPV1 channel activation[21-23], we found that $TRPV1^{CD4}$-mediated Ca^{2+} influx was almost completely abolished in the absence of Lck **(Fig. 4c)**. Collectively, these results suggest that TRPV1 is part of the proximal TCR

signaling cascade and that tyrosine phosphorylation by Lck is a possible gating mechanism of TRPV1^{CD4} after TCR stimulation.

We next evaluated the impact of TRPV1 deficiency on TCR signaling. We found no differences in phosphorylation of the TCR-proximal signaling components Zap70, Lat **(Fig. 4d)** or PLC-γ1 **(Fig. 4e)**, slight differences in Erk1/2 and p38 phosphorylation, and reduced Jnk activation in *Trpv1*$^{-/-}$ compared to WT CD4$^+$ T cells **(Fig. 4f)**. Consistent with the decreased TCR-induced Ca^{2+} influx, *Trpv1*$^{-/-}$ CD4$^+$ T cells failed to sustain NFAT-1 nuclear localization **(Fig. 4g)** and displayed reduced activation of NF-κB **(Fig. 4h)** upon TCR stimulation. Thus, TRPV1^{CD4} appears to be dispensable for proximal TCR signaling but it is required for the proper transduction of distal TCR signaling events.

TRPV1^{CD4} contributes to TCR-induced cytokine production

We reasoned that the altered TCR signaling in *Trpv1*$^{-/-}$ CD4$^+$ T cells would affect their subsequent cytokine production. We observed that *Trpv1*$^{-/-}$ CD4$^+$ T cells produced lower pan-cytokine levels (IFN-γ, IL-17A, IL-2, IL-10, IL-4 and TNF) after anti-CD3+28 stimulation compared to WT cells **(Fig. 5a)**. The opposite phenotype was observed for *Trpv1*^{Tg} CD4$^+$ T cells **(Supplementary Fig. 3a)**. The reduced cytokine production by *Trpv1*$^{-/-}$ CD4$^+$ T cells was not explained by increased apoptosis or a reduced proliferative response of these cells **(Supplementary Fig. 4)**. Moreover, TCR-independent activation of *Trpv1*$^{-/-}$ and WT CD4$^+$ T cells with PMA + ionomycin resulted in similar secretion of IFN-γ and IL-2 **(Fig. 5a, right panel)**. Using IL-2 as a readout, we found that its reduced production by *Trpv1*$^{-/-}$ CD4$^+$ T cells could be rescued by increasing the $[Ca^{2+}]_e$ in the culture medium **(Fig. 5b)**. These data suggest that the reduced cytokine production in *Trpv1*$^{-/-}$ CD4$^+$ T cells is likely due to the decreased TCR-induced Ca^{2+} influx observed in these cells **(Fig. 3** and **Supplementary Fig. 2)**. In addition, using an antigen-specific model, we found that *Trpv1*$^{-/-}$ OT-2 CD4$^+$ T cells stimulated by ovalbumin (OVA)-loaded WT DCs had a significantly reduced IFN-γ, IL-17A and IL-2 production compared to WT control OT-2 cells **(Fig. 5c** and **Supplementary Fig. 3b)**.

To further confirm the contribution of TRPV1^{CD4}-induced signaling to cytokine production, we treated WT CD4$^+$ T cells with BCTC. The TRPV1 antagonist concentration-dependently decreased CD4$^+$ T cell cytokine release upon stimulation with anti-CD3+28 Abs **(Fig. 5d)**. The observed decrease in cytokine production was not due to an increase in CD4$^+$ T cell apoptosis **(Fig. 5e)**. BCTC also significantly reduced cytokine production by OT-2 CD4$^+$ T cells upon stimulation with OVA-loaded DCs **(Fig. 5f)**. Taken together, these results suggest a cell-intrinsic role of TRPV1^{CD4} in promoting TCR-induced cytokine production.

TRPV1 inhibition decreases human CD4$^+$ T cell activation

To explore the relevance of the data generated in the mouse to the human system we determined the effect of TRPV1 pharmacological inhibition on the activation profile of primary CD4$^+$ T cells enriched from the peripheral blood of healthy donors. The cells were stimulated with anti-CD3+28 in the presence or absence of SB366791, a specific TRPV1 antagonist[12]. We analyzed the up-regulation of surface activation markers (i.e., CD25 and HLA-DR) 48h later and found that SB366791 concentration-dependently decreased their

expression **(Fig. 6a,b)**. Consistent with the murine system, TRPV1 inhibition also decreased IL-2 production **(Fig. 6c)**. Importantly, this effect was observed even at very low antagonist concentrations of the antagonist (≥ 0.01 μM) and was not associated with increased $CD4^+$ T cell apoptosis **(Fig. 6d)**. To confirm these findings, we performed siRNA-mediated knockdown of TRPV1 in primary human $CD4^+$ T cells. Similarly to TRPV1 pharmacological inhibition, TRPV1 knockdown decreases CD25 and HLA-DR up-regulation **(Fig. 6e,f)** and IL-2 production **(Fig. 6g,h)** upon anti-CD3+28 stimulation. Collectively, these data indicate the TRPV1 channel contributes to human $CD4^+$ T cell activation.

$TRPV1^{CD4}$ regulates proinflammatory $CD4^+$ T cell responses

To analyze the contribution of TRPV1-induced signaling to $CD4^+$ T cell responses *in vivo* we applied two different models of $CD4^+$ T cell-mediated colitis. We first used the $Il10^{-/-}$ model[25] and compared the severity of colitis in $Il10^{-/-}$ and $Il10^{-/-}Trpv1^{-/-}$ mice. $Il10^{-/-}$ mice lost more weight than $Il10^{-/-}Trpv1^{-/-}$ mice after induction and synchronization of the colitis by oral treatment with the non-selective COX inhibitor, piroxicam (PXC)[26] **(Fig. 7a)**. Histological analysis of the colons confirmed that $Il10^{-/-}$ mice developed severe inflammation with epithelial hyperproliferation, crypt loss and cellular infiltration in the mucosa and submucosa, whereas a significantly reduced inflammatory response was observed in $Il10^{-/-}Trpv1^{-/-}$ mice **(Fig. 7b-c)**. In addition, $Il10^{-/-}$ mice treated with the TRPV1 antagonist SB366791 showed attenuated colonic inflammation and T cell-derived inflammatory cytokine production compared to control, vehicle (VEH)-treated mice **(Supplementary Fig. 5)**.

To confirm the cell-intrinsic role of $TRPV1^{CD4}$ in intestinal inflammation, we transferred WT or $Trpv1^{-/-}$ naive ($CD4^+CD45RB^{hi}CD25^-$) T cells to $Rag1^{-/-}$ recipients and determined their ability to provoke colitis[25]. Recipients of WT naive $CD4^+$ T cells co-transferred with regulatory T (T_{reg}) cells ($CD4^+CD45RB^{lo}CD25^+$) were used as controls. Adoptive transfer of naive WT $CD4^+$ T cells induced severe colitis in the recipients as reflected by significant body weight loss, high disease activity index (DAI) and histological signs of severe colitis. This was not observed after the transfer of naive $Trpv1^{-/-}$ $CD4^+$ T cells **(Fig. 7d-g** and **Supplementary Fig. 6a,b)**. Massive cellular infiltration coinciding with severe crypt loss were evident in the colons of $Rag1^{-/-}$ mice transferred with WT naive $CD4^+$ T cells, but not with $Trpv1^{-/-}$ naive $CD4^+$ T cells **(Supplementary Fig. 6c)**. To quantify the amount of inflammatory cytokines produced in the colonic mucosa of these animals, we cultured *ex vivo* colonic explants (CEs). The CEs from $Rag1^{-/-}$ mice transferred with WT naive $CD4^+$ T cells released high amounts of IFN-γ, IL-17A and TNF as compared to CEs from recipients of $Trpv1^{-/-}$ naive $CD4^+$ T cells **(Fig. 7h)**. The mRNA levels of several proinflammatory cytokines (*Ifng, Il17a, Il22, Tnf* and *Il1b*) and chemokines (*Cxcl1, Cxcl9, Cxcl10, Ccl2* and *Ccl13*) were also decreased in colon homogenates from $Trpv1^{-/-}$ $CD4^+$ T cells recipients compared to WT $CD4^+$ T cell recipients **(Supplementary Fig. 6d)**. Transferred $Trpv1^{-/-}$ $CD4^+$ T cells secreted significantly lower amounts of proinflammatory cytokines (IFN-γ, IL-17A and TNF) compared to transferred WT $CD4^+$ T cells (**Fig. 7i**). Moreover, the numbers of IFN-γ, IL-17A and IL-10 producing $CD4^+$ T cells were also severely reduced in the spleen (SP), mesenteric lymph nodes (MLN) and the

lamina propria (LP) of the colitic recipients **(Supplementary Fig. 7)**, suggesting that the decreased colitogenicity of *Trpv1*$^{-/-}$ naive CD4^{+} T cells is possibly due to defective activation and differentiation *in situ*. In line with this hypothesis, we found that *Trpv1*$^{-/-}$ OT-2 naive CD4^{+} T cells had a decreased capacity to differentiate into T_H1, T_H2 and T_H17 effector cells *in vitro* compared to WT OT-2 naive cells **(Supplementary Fig. 8)**.

To analyze the potential contribution of TRPV1 in other cell types in the recipients, we compared the colitis induced by the transfer of WT naive CD4^{+} T cells in *Rag1*$^{-/-}$ to that induced in *Rag1*$^{-/-}$ *Trpv1*$^{-/-}$ recipients. We found that *Rag1*$^{-/-}$ and *Rag1*$^{-/-}$ *Trpv1*$^{-/-}$ recipients developed comparable body weight loss, colonic inflammation and displayed similar proinflammatory CD4^{+} T cell responses **(Fig. 8)**. Finally, in line with the increased activation profile *in vitro* **(Supplementary Fig. 3a)**, *Trpv1*^{Tg} naive CD4^{+} T cells induced an exacerbated colitis after transfer to *Rag1*$^{-/-}$ recipients **(Supplementary Fig. 9)**. Taken together, these results demonstrate an important cell-intrinsic role of TRPV1^{CD4} in promoting T cell activation and inflammatory responses (see Proposed model for the regulation of T-cell activation by TRPV1; **Supplementary Fig. 10**).

DISCUSSION

While CRAC channels have been described to be the major source for Ca^{2+} entry into T cells[1,3], several additional families of channels expressed on the plasma membrane of T cells may play important roles in this process, including Ca_V and TRP channels[2,5,6]. In particular, the contribution of TRP channels to this process is not well defined. TRP channels may decrease (e.g., TRPM4)[27] or increase (e.g., TRPC3)[7,28] Ca^{2+} influx in T cells and it is yet unclear whether they directly affect TCR signaling and T cell activation.

In the present study, we identified that the TRPV1 channel is functionally expressed in CD4^{+} T cells (TRPV1^{CD4}) and reported a novel function for TRPV1 beyond its well-recognized role as a pain receptor[10,29]. Our results indicate that TRPV1^{CD4} has an essential role in the activation and the acquisition of inflammatory properties by CD4^{+} T cells. TRPV1 expression was previously reported in peripheral blood lymphocytes in rat[30] and in human[7, 31-34], but the functionality of the TRPV1 channel was not assessed and it was unknown whether TRPV1 plays a role in T cell activation and function. In this study, we demonstrated that TRPV1 is constitutively expressed in mouse and human CD4^{+} T cells as well as in the Jurkat human leukemic T cell line. By employing the whole-cell patch clamp technique, we demonstrated the functionality of the TRPV1 channel at the plasma membrane and recorded capsaicin-evoked currents in WT but not in *Trpv1*$^{-/-}$ CD4^{+} T cells. The smaller TRPV1 current observed in CD4^{+} T cells compared to that previously reported in sensory neurons or in cells heterologously overexpressing TRPV1 might account for several cell-intrinsic factors: (i) a comparatively lower TRPV1 expression level in CD4^{+} T cells, (ii) different post-translational modifications (e.g., phosphorylation, glycosylation) that could increase TRPV1 activation threshold and result in a lower sensitivity to capsaicin; and/or (iii) the presence of different regulatory proteins associated with TRPV1^{CD4} (refs. 22,35,36). Nonetheless, it is well known that even small currents can produce physiologically significant increases in intracellular Ca^{2+} concentration and have profound consequences on cell physiology[37]. Accordingly, we identified by using Ca^{2+} imaging and

flow cytometry-based Ca^{2+} monitoring techniques that $TRPV1^{CD4}$ is a functional Ca^{2+} channel, and that it contributes to TCR-induced Ca^{2+} influx in a SOCE-independent manner. We also confirmed the contribution of TRPV1 to TCR-induced Ca^{2+} currents by whole-cell patch clamp and found that TCR-crosslinking produced significantly smaller inward currents in *Trpv1*$^{-/-}$ $CD4^+$ T cells compared to WT cells.

Our results suggest that TRPV1 is a component of the TCR signaling complex since it is rapidly recruited to TCR clusters upon TCR stimulation in a Src-dependent manner. Using a Jurkat cell clone that lack the expression of the Src-family kinase Lck[24], we identified that Lck rapidly tyrosine phosphorylates TRPV1 after TCR stimulation and regulates $TRPV1^{CD4}$ channel activity. Tyrosine phosphorylation by Src kinase has previously been shown to be essential for TRPV1 channel activation in other cell types. Indeed, capsaicin-induced currents in dorsal root ganglion (DRG) neurons are blocked by the Src-family kinase inhibitor PP2 and enhanced by the tyrosine phosphatase inhibitor sodium orthovandate. PP2 also abolished currents in HEK-293 cells transfected with rat TRPV1, whereas cotransfection of TRPV1 with v-Src resulted in fivefold increase in capsaicin-induced currents. Finally, in cells transfected with dominant-negative c-Src, capsaicin-induced currents were severely reduced[21,23]. This mode of activation by Src-family kinases is not restricted to TRPV1 and has also been shown for other TRP family members[22]. Our findings are therefore consistent with the previously reported TRPV1-Src protein-protein interaction and underline the role of Src-family kinases in the regulation of TRPV1 channel activity[21-23]. Tyrosine phosphorylation by Lck is therefore a possible gating mechanism of $TRPV1^{CD4}$ after TCR stimulation.

The analysis of TCR signaling in WT and *Trpv1*$^{-/-}$ $CD4^+$ T cells revealed a reduced activation of the p38 and Jnk pathways and a clear decrease in nuclear translocation of NF-κB in *Trpv1*$^{-/-}$ $CD4^+$ T cells. In line with the decreased TCR-induced Ca^{2+} influx, *Trpv1*$^{-/-}$ $CD4^+$ T cells also failed to maintain nuclear localization of NFAT-1 after TCR stimulation. Consequently, *Trpv1*$^{-/-}$ $CD4^+$ T cells display a significantly reduced cytokine production profile upon antigen-specific (OVA-loaded DCs) and nonspecific (anti-CD3+28) stimulation. Collectively, these data indicate that TRPV1 is necessary for proper TCR-induced signaling and cytokine production but dispensable for $CD4^+$ T cell proliferation under our experimental conditions.

Consistent with our *in vitro* data, we found that $TRPV1^{CD4}$ plays an important role in T cell inflammatory responses *in vivo*, in two different models of inflammatory bowel disease (IBD). *Il10*$^{-/-}$ *Trpv1*$^{-/-}$ and TRPV1 antagonist-treated *Il10*$^{-/-}$ mice displayed reduced colonic inflammation compared to untreated *Il10*$^{-/-}$ controls. In addition, *Trpv1*$^{-/-}$ naive $CD4^+$ T cells had an impaired capacity to provoke colitis when transferred to *Rag1*$^{-/-}$ recipients. As the activation of TRPV1 in sensory afferents contributes to neurogenic inflammation, which could affect colitis severity[38], we compared the colitis induced by the transfer of WT naive $CD4^+$ T cells in *Rag1*$^{-/-}$ to those induced in *Rag1*$^{-/-}$ *Trpv1*$^{-/-}$ mice. The genetic deletion of TRPV1 in donor $CD4^+$ T cells, but not in other cells of the recipients, determined the severity of colonic inflammation in this model. The T cell-intrinsic role of TRPV1 was further demonstrated by the increased activation profile and proinflammatory properties of *Trpv1*^{Tg} $CD4^+$ T cells.

Finally, our results indicate that inhibition of $TRPV1^{CD4}$ in mouse and human $CD4^+$ T cells with TRPV1 antagonists or with TRPV1 siRNA, recapitulate the phenotype of *Trpv1*$^{-/-}$ $CD4^+$ T cells. As TRPV1 functions as a nociceptor (i.e., pain receptor) in sensory neurons[29], TRPV1 antagonists were developed as analgesic agents[39]. The immunomodulatory properties of TRPV1 antagonists identified in this study suggest that their application might be beneficial in patients with $CD4^+$ T cell-mediated immunopathologies such as IBD.

ONLINE METHODS

Reagents and Antibodies

For immunoblotting, we used: anti-phospho Erk1/2 (D13.14.4E), p38 (D3F9), and Jnk (81E11), and anti-total Erk1/2 (137F5), p38 (#9212), Jnk (#9252) Abs; anti-phospho Zap70 (Tyr319) and PLC-γ1 (Tyr783) Abs (Cell Signaling Technology), anti-phospho Lat (Tyr191) and anti-p-Tyr (4G-10) Abs (Millipore); Anti-CD3ε (M-20; sc-1127), anti-Lck (2102; sc-13) and anti-TRPV1 (P-19; sc-12498) Abs (Santa Cruz Biotechnology); anti-TRPV1 (#ACC-030, Alomone), anti-NFAT1 mAb (ab2722, Abcam), and anti-β-actin (AC-74, Sigma). For immunofluorescence studies, anti-TRPV1 (sc-12498) and anti-Lck (sc-13) (Santa Cruz Biotechnology), anti-CD4 (GK1.5, eBioscience), anti-CD45 and anti-Claudin-3 Abs (BD Biosciences). For T cell stimulation, anti-mouse CD3ε (145-2c11) and anti-mouse CD28 (PV-1) (BioXcell), and anti-human CD3ε (UCHT1) and anti-human CD28 (CD28.2) (eBioscience) mAbs were used; PMA (Phorbol 12-myristate 13-acetate), ionomycin, thapsigargin and phytohemagglutinin were from Sigma; The Src-family kinase inhibitor PP2 was from Cayman Chemical, the TRPV1 antagonists were from Tocris (BCTC, I-RTX) and Enzo Life Sciences (SB366791), the Annexin-V/7-AAD apoptosis detection kit was from BD Biosciences and CFSE, Indo-1 AM, and Fura-2 AM were from Invitrogen/Molecular Probes.

Mice

Six to ten week old mice were used for all the experimental procedures. Specific pathogen free C57BL/6 (B6) mice were purchased from Harlan Sprague Dawley or bred in our vivarium. *Trpv1*$^{-/-}$[29], *Trpv3*$^{-/-}$[41], *Rosa26-Trpv1*[13], *Cd4*-Cre, *Rag1*$^{-/-}$ and OVA-transgenic (OT-2) mice on the B6 background (all from the Jackson Laboratories) were bred in our animal facility. To generate *Trpv1*$^{-/-}$ OT-2, *Il10*$^{-/-}$ *Trpv1*$^{-/-}$ and *Rag*$^{-/-}$ *Trpv1*$^{-/-}$, *Trpv1*$^{-/-}$ mice were intercrossed with OT-2, *Il10*$^{-/-}$ or *Rag1*$^{-/-}$ mice respectively. Mice with CD4-Cre driven expression of a TRPV1 (*Trpv1*^{Tg}) transgene were generated by crossing mice harboring alleles for *ROSA-stop*^{flox}*-TRPV1-IRES-ECFP* (*Rosa26-Trpv1*) and *Cd4*-Cre in our vivarium. Mice were bred for more than 6 months in our vivarium and were genotyped before they were used in any experiments. All experimental procedures were conducted in accordance with UCSD institutional guidelines for animal care and use.

Isolation and stimulation of $CD4^+$ T cells

Mouse $CD4^+$ T cells were isolated from the SP or MLN using a $CD4^+$ T cell negative selection kit (StemCell #19752). Purity of the enriched populations was controlled by FACS staining for CD4 and TCRβ and was typically >94% for spleen and >97% for MLN derived $CD4^+$ T cells. For ELISA, $CD4^+$ T cells were stimulated with 10 μg/mL plate-bound anti-

CD3 and 1 μg/mL soluble anti-CD28 Abs in complete RPMI 1640. Twenty-four and 48h culture supernatants were collected for cytokine production analysis (ELISA kits, eBioscience). For signaling experiments, $CD4^+$ T cells were stimulated with 5 μg/mL anti-CD3 and 2 μg/mL anti-CD28 Abs (both soluble) for the indicated time-points (e.g., 0, 15, 30, 60 min). SP $CD4^+$ T cells from TCR transgenic mice (OT-2 or *Trpv1*$^{-/-}$ OT-2) were isolated as described above. Bone marrow-derived dendritic cells (BMDCs) were cultured and harvested as previously described[42]. $CD11c^+$ BMDCs or splenic DCs (SPDCs) were isolated using a $CD11c^+$ positive selection kit (StemCell #18758) and then loaded with 10 μg/mL of I-Ad-restricted OVA peptide ($OVA_{323-339}$: ISQAVHAAHAEINEAGR, PeptidoGenic Research) for 2h before the addition of WT or *Trpv1*$^{-/-}$ OT-2 $CD4^+$ T cells to the culture (DC/T cell ratio of 1:2). After five days of co-culture, $CD4^+$ T cells were recovered and re-stimulated with anti-CD3+28 Abs for 24h. Supernatants were then collected and cytokines levels measured by ELISA. For experiments on primary human $CD4^+$ T cells, peripheral blood mononuclear cells (PBMCs) were isolated by Ficoll density gradient technique from healthy blood donors. For some experiments, $CD4^+$ T cells have been isolated from the PBMCs and expanded with phytohemagglutinin and allogeneic irradiated feeder cells (1×10^5/well) as previously described[43]. The $CD4^+$ T cell clones or the PBMCs were treated or not with indicated concentrations of a TRPV1 antagonist (SB366791) and stimulated with anti-hCD3 and anti-hCD28 Abs (both 1 μg/mL soluble) in complete RPMI 1640 for 48h. For TRPV1 phosphorylation analysis by immunoblot, Jurkat T cells (clones E6.1 and J.Cam1.6) were purchased from the ATCC, grown in complete RPMI 1640 and stimulated with soluble anti-hCD3 (OKT3; Biolegend; 2.5 μg/mL) and anti-hCD28 Abs (1 μg/mL; eBioscience) for the indicated amount of time.

TRPV1 knockdown

Primary human $CD4^+$ T cell clones or freshly isolated PBMCs were transfected with 400 nM of TRPV1 siRNA (sc-36826, Santa Cruz Biotechnology, a pool of 3 different siRNA duplexes) or control siRNA (Non-Targeting siRNA #1; Dharmacon) at a cell density of 5×10^6 cells per 100 μL of human T cell nucleofector solution (kit VPA-1002; Lonza) with the Amaxa Nucleofector II device using program U-014 (Lonza). After nucleofection, cells were immediately transferred into prewarmed complete RPMI 1640 and cultured in a 24-well plate at 37 °C in a 5% CO2 humidified incubator. Six hours after transfection cells were stimulated with anti-hCD3 and anti-hCD28 Abs as described above for a further 42h. Cells were then analyzed for TRPV1 knockdown efficiency (FACS, IB), up-regulation of surface activation markers (CD25 and HLA-DR; FACS) and cytokine production (IL-2; ELISA). To knockdown TRPV1 in Jurkat T cells (clone E6.1), cells were stably transduced with TRPV1 shRNA lentiviral particles (sc-36826-V) or with copGFP control lentiviral particles (sc-108084) according to manufacturer's instructions (Santa Cruz Biotechnology). TRPV1 knockdown efficiency was evaluated by immunoblotting and Ca^{2+} imaging after 7-10 days of selection with puromycin (2 μg/mL).

In vitro T cell differentiation

$CD4^+CD25^-$ (naive) T cells were isolated from the spleen of WT OT-2 or *Trpv1*$^{-/-}$ OT-2 mice and co-cultured (1×10^6 cells/well) with OVA-loaded (10 μg/mL $OVA_{323-339}$ peptide for 24h at 37°C) γ-irradiated (3000 rad from a ^{137}Cs source) BMDCs (5×10^5 cells/well) in flat-

bottom 24 well plates in complete RPMI medium (unless indicated otherwise) in presence of: recombinant murine (rm) IL-12 (10 ng/mL) and neutralizing anti-IL-4 Ab (10 μg/mL) for Th1; rm IL-4 (10 ng/mL), neutralizing anti-IFN-γ and anti-IL-12 Abs (both at 10 μg/mL) for Th2; rm IL-6 (20 ng/mL) and TGF-β (4 ng/mL), neutralizing anti-IFN-γ and anti-IL-4 Abs (both at 10 μg/mL) in complete IMDM medium; rm TGF-β (10 ng/mL) and IL-2 (20 ng/mL) for T_{reg} differentiation. At day 2, rm IL-2 (10 ng/mL) was added into the Th1 and Th2 cultures. After 4 days, $CD4^+$ T cells were recovered and re-stimulated or not with 10 μg/mL plate-bound anti-CD3 and 1 μg/mL soluble anti-CD28 Abs in the presence of GolgiStop (BD Biosciences) for 5 hours. Measurement of intracellular cytokine production was performed using antibodies to IFN-γ, IL-4, IL-17A and IL-10 according to the manufacturer's instructions (eBioscience).

CFSE Proliferation Assay

Isolated splenic $CD4^+$ T cells were suspended in PBS/2% FBS at 10×10^6 cells/mL. A 100 μM working dilution was prepared in PBS/2% FBS from the CFSE stock solution (5 mM in DMSO). CFSE was added to the cells at a final concentration of 1 μM and the cells were incubated at 37°C for 7 min. Incorporation of CFSE into cell membranes was stopped by adding 5 volumes of ice-cold RPMI supplemented with 30% FBS. Excess CFSE was removed by three successive media washes. Dilution of CFSE in dividing cells was monitored 72h after stimulation with anti-CD3+28 Abs or PMA+ionomycin as described above and was assessed by FACS on gated $CD4^+$ T cells.

Electrophysiological Assays

Whole-cell patch clamp recording and analysis were carried out on an Axopatch 200B amplifier with Digidata1322A interface and pClamp9 software (Axon Instruments). Patch electrodes were pulled from thin-walled borosilicate glass (World Precision Instruments) on a horizontal micropipette puller (Sutter Instruments). Electrodes had a resistance of 8-20 MΩ when filled with intracellular solution. Analog capacity compensation and series resistance compensation were used during whole-cell recordings. For single pulse recordings, SP $CD4^+$ T cells were held either at −85 mV and capsaicin (CAP, 16 μM) was introduced via a gravity-fed perfusion system into the recording chamber using a TC344B heater controller and an SH-27B inline heater (Warner instruments). For experiments performed in the presence of SB366791, cells were pretreated for 30 min in external solution containing 1 μM of SB366791, and currents were then recorded in the presence of both capsaicin (16 μM) and SB366791 (1 μM). For TCR stimulation, cells were first pretreated with biotinylated anti-CD3 Ab (20 μg/mL) for 20 min at 4°C, and then they were activated by adding streptavidin (10 μg/mL) in the external solution and were held at −85 mV. Data were sampled at 10 kHz, and filtered at 5 kHz, and whole-cell recordings were performed at 35°C. The extracellular solution contained (in mM): 144 NaCl, 5 KCl, 2 MgCl2, 1 CaCl2, 10 glucose, 10 HEPES, and was adjusted to pH 7.4 with NaOH. The intracellular solution used in the pipettes contained (in mM): 126 K-gluconate, 10 KCl, 5 EGTA, 4 MgATP, 10 HEPES, and was adjusted to pH 7.4 with KOH. For I-V relationships, the external solution contained (in mM): 140 NaCl, 5 KCl, 2 MgCl2, 5 EGTA, 10 HEPES, 10 glucose, and was adjusted to pH 7.2 with NaOH. The internal solution contained (in mM): 136 CsCl, 5 EGTA,

10 HEPES, 4 MgATP, and was adjusted to pH 7.4 with NaOH. Liquid junction potential was calculated at +15 mV and was corrected offline.

Single-Cell Ca^{2+} Imaging

Naive $CD4^+$ T cells were isolated from the spleen of WT, *Trpv1*$^{-/-}$ or *Trpv1*^{Tg} mice, loaded with 1 μM Fura-2/AM (Molecular Probes) in culture medium (1×10^6 cells/mL) for 30 min at 22-25°C, washed and attached to poly-D-lysine-coated coverslips for 15 min. For $[Ca^{2+}]_i$ measurements, coverslips were mounted on a RC-20 closed-bath flow chamber (Warner Instrument Corp.) and analyzed on an Olympus IX51 epifluorescence microscope with Slidebook (Intelligent Imaging Innovations, Inc.) imaging software as described previously[44]. Store-operated Ca^{2+} measurements were performed after passive depletion of intracellular stores using 1 μM thapsigargin. For TCR stimulation, cells were first pretreated with 5 μg/mL of biotinylated anti-CD3 Ab (clone 145-2C11, eBioscience) and anti-CD3 crosslinking was performed using 10 μg/mL of immuno pure streptavidin (Pierce). For measurement of TRPV1 activity, cells were perfused with Ringer solution containing 1 or 10 μM of capsaicin. Fura-2 emission was detected at 510 nm with excitation at 340 and 380 nm and Fura-2 emission ratio (340 / 380) was acquired every 5-s interval after background subtraction. For each experiment, 50-100 individual cells were analyzed using OriginPro (Originlab) analysis software. For $[Ca^{2+}]_i$ measurements in Jurkat T cells, the Fura-2 fluorescence ratios were collected on a Nikon microscope stage equipped with a 40X Nikon UV-Fluor objective and an intensified CCD camera (ICCD200). The fluorescence signals emitted from the cells were monitored continuously in 5-s intervals using a MetaFluor Imaging System (Universal Imaging) and recorded for later analysis. Peak or sustained Ca^{2+} ratios were calculated as the maximal amount of Ca^{2+} accumulated in the cell after baseline subtraction (before addition of Ca^{2+} containing Ringer's solution), upon reintroduction of Ca^{2+} containing Ringer's solution. All experiments were performed at room temperature (22-25°C).

Ca^{2+} Flux Measurement by Flow Cytometry

$CD4^+$ T cells were isolated from the spleen of WT, *Trpv1*$^{-/-}$, *Trpv1*^{Tg} or *Trpv3*$^{-/-}$ mice and $[Ca^{2+}]_i$ was measured as previously described[45, 46]. Briefly, cells were suspended at 2.5×10^6/mL in PBS/2% FBS and pre-labeled with CFSE (carboxyfluorescein diacetate succinimidyl ester, Molecular Probes; 40 nM, for 10 min at 37°C) or were mock-treated and mixed at equal proportion [e.g., WT cells (CFSE) plus *Trpv1*$^{-/-}$ cells (mock)]. In some experiments, the CFSE- and mock-treated pairs were reversed to ensure that the CFSE staining did not alter the results. Cells were washed, resuspended at 5×10^6/mL in PBS/2% FBS and incubated with 2 μM Indo-1 AM (Molecular Probes) for 30 min at 37°C, 5% CO_2. Cells were then washed, stained with CD4-APC Ab (eBioscience) and resuspended at 1×10^6 cells/mL in complete RPMI. Finally, cells were transferred to calcium-free medium (Ca^{2+} and Mg^{2+}-free Hank's balanced-salt solution [HBSS] supplemented with 2% FCS and 1 mM EGTA) just before the beginning of the acquisition. Cells were pre-incubated or not with indicated concentrations of TRPV1 antagonists (BCTC or I-RTX) or with the vehicle (0.1% DMSO) for 5 min at 37°C and stimulated at 37°C with 1 or 10 μM capsaicin, 10 μg/mL anti-CD3 and 1 μg/mL anti-CD28 Abs or alternatively with 500 nM of ionomycin or 1 μM thapsigargin. Indicated concentrations of $CaCl_2$ were added during the analysis on a BD

LSRII flow cytometer. The data are presented as the ratio of Indo-1 fluorescence violet (405 nm) / blue (510 nm) and were calculated on gated $CD4^+$ cells using FlowJo (TreeStar).

Flow Cytometry Analysis

For surface markers staining, mouse and human $CD4^+$ T cells were stained with anti-mouse CD4-APC, CD25-AF488, CD45RB-PE and TCRβ-PerCP-Cy5.5 Abs or with anti-human CD4-PerCP-Cy5.5, CD25-PE and HLA-DR-FITC Abs (all from eBioscience) respectively for 30 min at 4°C. For intracellular staining, cells were fixed in 2% paraformaldehyde/PBS for 10 min at room temperature, centrifuged and permeabilized in 0.2% Triton X-100 (TRPV1 staining) or in ice cold 100% methanol (phospho [p]-PLC-γ1 staining) for 15 min at 4°C. For TRPV1 staining, cells were then washed, blocked with 5% BSA in PBS for 30 min at 4°C and stained with an anti-TRPV1 goat Ab (sc-12498, preincubated or not for 2h at RT with 10-fold excess of the specific blocking peptide) or normal goat IgG (sc-2028) as control for 1h at 4°C. For p-PLC-γ1 intracellular staining, cells were incubated with anti-mouse CD16/CD32 mAb 2.4 G2 (Fc Block, BD Biosciences) and stained with anti-p-PLC-γ1 Ab (Cell Signaling) for 30 min at 4°C. All primary Abs were used at 1:100 dilution unless indicated otherwise. Cells were then washed and incubated for 30 min at 4°C with anti-mouse CD4-APC and TCRβ-PerCP-Cy5.5 Abs together with anti-rabbit-AF-488 (p-PLC-γ1 staining) or with anti-goat-AF-488 (TRPV1 staining) secondary Abs (both 1:500 dilution; Invitrogen). Cells were finally washed and analyzed on a BD FACSCalibur or Accuri C6 flow cytometers. The data were analyzed using FlowJo software (TreeStar).

Immunofluorescent Stainings and Confocal Microscopy Analysis

SP $CD4^+$ T cells were isolated as described above and cytocentrifuged (Cytospin 2, Shandon) onto microscope slides for 3 min at 500 r.p.m. Alternatively, Chinese Hamster Ovary (CHO) control or overexpressing rat TRPV1 were grown on collagen type 1-coated coverslips (BD Biosciences) for 1-2 days in complete DMEM-F12 supplemented (CHO-TRPV1) or not (CHO-control) with Geneticin (1.2 mg/mL). The air-dried cytospin preparations or the coverslips were fixed in 4% paraformaldehyde/PBS for 10 min at room temperature and permeabilized in 0.2% Triton X-100 for 15 min at 4°C. Cells were then washed, blocked with 5% BSA / 0.2% Triton X-100 in PBS for 30 min at 4°C and stained with an anti-TRPV1 goat Ab (sc-12498) or with normal goat IgG (sc-2028) for 1h at 4°C. The cells were washed and incubated for 30 min at 4°C with an anti-CD4-AF-488 Ab (eBioscience) and an anti-goat-AF-546 secondary Ab (Invitrogen). For TCR clustering experiments, SP $CD4^+$ T cells were pretreated or not with the Src-family kinase inhibitor PP2 (10 μM) for 1h at 37°C before being incubated on ice with a hamster anti-CD3ε Ab (20 μg/mL soluble) for 30 min. The cells were washed, stained with an anti-hamster AF-488 secondary Ab (Invitrogen) on ice and in the dark for 30 min, and left unstimulated or stimulated for 5 min at 37°C. Cells were stained for TRPV1 as described above and for Lck with an anti-p56Lck rabbit Ab (Santa Cruz sc-13 Ab; 1h at 4°C) and with a secondary anti-rabbit-AF-647 Ab (Invitrogen; 30 min at 4°C). All the primary and secondary Abs were used at 1:100 dilution unless indicated otherwise. One cytospin preparation served as a negative control staining using the control IgGs or the secondary Abs only. Cells were finally stained 10 min at RT with Hoechst 33342 (50 ng/mL, Invitrogen), rinse with deionized water and slides were mounted in ProLong Gold antifade reagent (Invitrogen).

The fluorescence images were acquired using a 100× oil immersion objective on a confocal laser-scanning microscope (Olympus IX81) with Fluoview software. Colocalization studies were performed using Velocity® software.

Electrophoretic-Mobility Shift Assay (EMSA), Immunoprecipitation (IP) and Immunoblotting (IB)

For assessment of nuclear translocation of NF-κB and NFAT-1 in WT and *Trpv1*$^{-/-}$ SP CD4^{+} T cells, cytoplasmic cell extracts were made by lysis in hypotonic lysis buffer A (10 mM HEPES [pH 7.9], 10 mM KCl, 0.1 mM EDTA, complete protease inhibitors [Roche]) for 5 minute incubation on ice. After collecting the cytoplasmic extracts, the cell pellet was lysed in nuclear extract buffer B (20 mM HEPES [pH 7.9], 420 mM NaCl, 1 mM EDTA, protease inhibitors) on ice for 5 min on ice. Translocation of activated NF-κB into the nucleus was measured by EMSA using consensus NF-κB oligonucleotides (Santa Cruz Biotechnologies) as previously described[42]. Translocation of NFAT-1 was analyzed in the nuclear fractions by immunoblotting using a mouse anti-NFAT-1 mAb (Abcam). The phosphorylation of Zap70, Lat, Erk, p38 and Jnk was assessed in the cytosolic fraction using specific Abs for phospho and total forms of these proteins (Cell Signaling). The protein concentration was determined with a protein-quantification kit (Bio-Rad). Protein samples (10 μg/lane) were separated through SDS polyacrylamide gel electrophoresis (4-12% acrylamide NuPAGE Novex bis-Tris precast gels; Life Technologies) and then transferred to PVDF membranes (Millipore). The blots were blocked by 5% BSA/0.3% Tween 20 in PBS for 45 min at RT, and incubated with primary Abs (all Abs were used at 1:1000 dilution) overnight at 4°C. The blots were washed and incubated with their corresponding HRP-conjugated secondary Abs from Sigma or Jackson Lab (1:5000 to 1:10000 dilution) for 45 min at RT and developed in ECL solution (Pierce). Quantification of IB results by band densitometry analysis was performed with Image J software. To measure TRPV1 expression by IB, resting mouse and human primary CD4^{+} T cells, Jurkat T cells, CHO-control and −TRPV1+ were lysed with RIPA buffer (Teknova) supplemented with protease inhibitors (Roche) and IB analysis was performed as described above using anti-TRPV1 Abs (sc-12498, Santa Cruz, 1:1000 dilution or ACC-030, Alomone, 1:200 dilution). For analysis of TRPV1 tyrosine phosphorylation, resting or anti-CD3+28 Abs stimulated WT and *Lck*$^{-/-}$ Jurkat T cells were lysed with RIPA buffer supplemented with protease inhibitors (Roche) and TRPV1 IPs were carried out on cleared lysates overnight at 4 °C with an anti-TRPV1 goat Ab (sc-12498; Santa Cruz) coupled to protein A magnetic beads (New England Biolabs). Normal goat IgG was used as negative control (sc-2028; Santa Cruz). After IP, the immunoprecipitates were washed three times with the lysis buffer and then subjected to SDS-PAGE. The blots were probed with anti-p-Tyr, anti-TRPV1 and anti-Lck Abs and developed as described above.

Biotinylation of Cell Surface Proteins

Cell surface proteins of Jurkat T cells were biotinylated and immunoprecipitated using a cell surface protein isolation kit from Pierce (Thermo Scientific #89881) according to manufacturer's instructions. Briefly, 25×10^{6} Jurkat T cells GFP (control) or TRPV1 knockdown (*Trpv1*^{KD}) were biotinylated with 0.25 mg/mL solution of EZ-Link Sulfo-NHS-SS-Biotin in PBS for 30 min at 4°C under gentle agitation. After quenching of the reaction

and cell lysis, the biotinylated proteins were isolated by NeutrAvidin agarose beads (Pierce) and eluted from the beads by incubation for 60 min at RT in SDS-PAGE Sample Buffer (62.5 mM Tris-HCl, pH 6.8, 1% SDS, 10% glycerol, 50 mM of DTT). A sample of the initial cell lysates was retained for analysis of total proteins. Proteins were resolved by SDS polyacrylamide gel electrophoresis as described in the immunoblotting section of the Methods.

Isolation of mRNA and qPCR

Isolation of RNA was carried out with the RNeasy Mini Kit (Qiagen) following the manufacturers protocol. One μg of RNA sample was used for reverse transcription and synthesis of cDNA using qScript cDNA superMix (Quanta Biosciences). Quantitative real-time PCR (qPCR) was performed on an AB7300 (Applied Bisosytems) using PerfeCTa SYBR Green FastMix (Quanta Biosciences). Primers for specific target genes were designed based on their reported sequences and synthesized by IDT Technologies (see Supplementary Table 1 and 2 for primer sequences). The comparative expression of several *Trp* channels in murine $CD4^+$ T cells was performed after verifying that amplification efficiencies for the different target genes were comparable. For TRPV1 expression analysis, qPCR products were run on a 2% agarose gel stained with SYBR Safe DNA (Invitrogen) to further confirm the specificity of the primers used.

Il10$^{-/-}$ Model of Colitis

Eight to 10 week old sex and age-matched *Il10*$^{-/-}$ or *Il10*$^{-/-}$ *Trpv1*$^{-/-}$ mice were randomly assigned to the different groups. In order to overcome the variability in severity and onset of the disease in this model, colitis was induced by treatment with the non-steroidal anti-inflammatory drug (NSAID) Piroxicam[26] (PXC, Sigma). Mice were fed with normal chow mixed or not with PXC for 14 consecutive days (50 mg/250g of food the 1^{rst} week and 70 mg/250g of food the 2nd week). In some experiments, *Il10*$^{-/-}$ mice were treated daily with the TRPV1 antagonist SB366791 (3 mg/kg of body weight, i.p) or with its vehicle (10%DMSO/90%Saline) starting 3 days prior and daily during the 14 days of the colitis induction by PXC. Wasting disease in the different groups was monitored periodically and mice were sacrificed at day 30 for analysis.

T cell Adoptive Transfer Model of Colitis

SP naive $CD4^+$ T cells isolated from WT, *Trpv1*$^{-/-}$ or *Trpv1*^{Tg} donor mice were adoptively transferred to *Rag1*$^{-/-}$ or *Rag1*$^{-/-}$ *Trpv1*$^{-/-}$ recipients as previously described[47,48]. Briefly, $CD4^+$ T cells were enriched by immunomagnetic negative selection, stained with CD4-APC, CD25-AF488 and CD45RB-PE (eBioscience) and sorted into naive $CD4^+CD45RB^{high}CD25^-$ and regulatory $CD4^+CD45RB^{low}CD25^+$ populations (usual purity >98%) with a BD FACSAria II Flow Cytometer. Eight to 10 week old *Rag1*$^{-/-}$ or *Rag1*$^{-/-}$ *Trpv1*$^{-/-}$ sex and age-matched recipients were reconstituted by i.p. injection with 3×10^5 naive $CD4^+$ T cells from WT, *Trpv1*$^{-/-}$ or *Trpv1*^{Tg} sex-matched donor mice. For the co-transfer experiments, 1.5×10^5 regulatory T cells from WT mice were co-injected with the naive $CD4^+$ T cell population. After reconstitution, mice were monitored weekly for signs of intestinal inflammation such as weight loss and diarrhea. The DAI (the combined score of

weight loss and bleeding) was determined as previously described[47, 48]. Diseased animals were sacrificed for analysis as indicated.

Isolation of lamina propria lymphocytes (LPLs)

Isolation of LPLs was performed as previously described[47]. Briefly, colons were washed with PBS and cut into small pieces (≈1-2 mm). The tissue pieces were digested with PBS containing 0.5 mg/ml of collagenase IV and 0.5 mg/ml of DNase I (both from Sigma) for 2 × 30 min at 37°C under rotation. The cell suspension containing LPLs was collected through a 40 μm cell strainer. Finally, the LPLs were isolated by centrifugation with 40/80 Percoll (GE healthcare) gradient for 20 min at 1,000g at 20°C without brake (usual $CD4^+$ T cell purity > 80%).

Colonic Explants (CE)

Colonic longitudinal sections (3-4 mm wide) were weighed and washed in RPMI medium 1640 containing 100 μg/ml streptomycin and 100 U/ml penicillin. The CE were cultured for 24h in complete RPMI 1640 at 37°C and 5% CO_2. Culture supernatants were then collected and cytokine levels measured (ELISA).

Histological Analysis

Entire colons were excised, opened longitudinally, rolled onto a wooden dowel and fixed with 10% buffered formalin. Paraffin sections (5 μm) were stained with H&E. Colonic epithelial damage was scored blindly as follows: 0 = normal; 1 = hyperproliferation, irregular crypts, and goblet cell loss; 2 = mild to moderate crypt loss (10-50%); 3 = severe crypt loss (50-90%); 4 = complete crypt loss, surface epithelium intact; 5 = small to medium sized ulcer (<10 crypt widths); 6 = large ulcer (>10 crypt widths). Infiltration with inflammatory cells was scored separately for mucosa (0 = normal; 1 = mild; 2 = modest; 3 = severe), submucosa (0 = normal; 1 = mild to modest; 2 = severe), and muscle/serosa (0 = normal; 1 = moderate to severe). Scores for epithelial damage and inflammatory cell infiltration were added, resulting in a total colitis scoring range of 0-12.

Statistical Analysis

Data are presented as mean ± SEM. The statistical significance between two groups was determined using unpaired Student t-test with two-tailed p-values. The statistical significance between more than two groups was determined using one-way ANOVA with post hoc Dunnett's or Bonferroni tests. For time course experiments *in vivo*, two-way ANOVA with post hoc Bonferroni test was used. All statistics were performed using PRISM software (GraphPad Software).

Supplementary Material

Refer to Web version on PubMed Central for supplementary material.

ACKNOWLEDGMENTS

We thank C. Conche and K. Sauer for help with measurements of Ca^{2+}; A. Patapoutian (The Scripps Research Institute) for Chinese hamster ovary cells transfected to express TRPV1; E. Garcia and T. Snutch (University of

British Columbia) for access to electrophysiological equipment; J. Lee and C. Quinley for discussions; M. Scholl for animal breeding; T. Rambaldo for cell sorting; S. Shenouda for tissue processing; N. Varki and L. Eckmann for help with histological evaluations; and J. Santini of the Neuroscience microscopy shared facility, funded by NINDS, NIH, grant P30 NS047101, for technical assistance with confocal imaging. Supported by the US National Institutes of Health (U01 AI095623 and P01 DK35108 to E.R., and AI083432 to Y.G.), the Canadian Institutes of Health Research (MOP-102698 to W.A.J.), the Broad Foundation (IBD-0342R to E.R.), the Crohn's & Colitis Foundation of America (SRA 3038 to E.R., RFA 3574 to S.B., and RFA 2927 to P.R.d.J.), the European Molecular Biology Organization (ALTF 288-2009 to S.B.), the Fulbright Association (S.B.), the Philippe Foundation (S.B.) and the Japan Society for the Promotion of Science (Y.A.-N.).

Non-standard abbreviations

$[Ca^{2+}]_e$	extracellular calcium concentration
$[Ca^{2+}]_i$	intracellular calcium concentration
CAP	capsaicin
Ca_V	voltage-gated Ca^{2+} channels
CE	colonic explants
CRAC	Ca^{2+} release-activated Ca^{2+} channel
DAI	Disease Activity Index
Iono	ionomycin
LP	lamina propria
MLN	mesenteric lymph nodes
SOCE	store-operated calcium entry
SP	spleen
TG	thapsigargin
TRPV1	Transient Receptor Potential cation channel, subfamily V, member 1

REFERENCES

1. Oh-hora M, Rao A. Calcium signaling in lymphocytes. Curr. Opin. Immunol. 2008; 20:250–258. [PubMed: 18515054]
2. Gallo EM, Cante-Barrett K, Crabtree GR. Lymphocyte calcium signaling from membrane to nucleus. Nat. Immunol. 2006; 7:25–32. [PubMed: 16357855]
3. Hogan PG, Lewis RS, Rao A. Molecular basis of calcium signaling in lymphocytes: STIM and ORAI. Annu. Rev. Immunol. 2010; 28:491–533. [PubMed: 20307213]
4. Omilusik K, et al. The Ca(v)1.4 calcium channel is a critical regulator of T cell receptor signaling and naive T cell homeostasis. Immunity. 2011; 35:349–360. [PubMed: 21835646]
5. Omilusik KD, Nohara LL, Stanwood S, Jefferies WA. Weft, warp, and weave: the intricate tapestry of calcium channels regulating T lymphocyte function. Front. Immunol. 2013; 4:164. [PubMed: 23805141]
6. Schwarz EC, et al. TRP channels in lymphocytes. Handb. Exp. Pharmacol. 2007; (179):445–456. [PubMed: 17217072]
7. Wenning AS, et al. TRP expression pattern and the functional importance of TRPC3 in primary human T cells. Biochim. Biophys. Acta. 2011; 1813:412–423. [PubMed: 21215279]
8. Venkatachalam K, Montell C. TRP channels. Annu. Rev. Biochem. 2007; 76:387–417. [PubMed: 17579562]

9. Owsianik G, Talavera K, Voets T, Nilius B. Permeation and selectivity of TRP channels. Annu. Rev. Physiol. 2006; 68:685–717. [PubMed: 16460288]
10. Caterina MJ, et al. The capsaicin receptor: a heat-activated ion channel in the pain pathway. Nature. 1997; 389:816–824. [PubMed: 9349813]
11. Touska F, Marsakova L, Teisinger J, Vlachova V. A “cute” desensitization of TRPV1. Curr. Pharm. Biotechnol. 2011; 12:122–129. [PubMed: 20932251]
12. Gunthorpe MJ, et al. Identification and characterisation of SB-366791, a potent and selective vanilloid receptor (VR1/TRPV1) antagonist. Neuropharmacology. 2004; 46:133–149. [PubMed: 14654105]
13. Arenkiel BR, Klein ME, Davison IG, Katz LC, Ehlers MD. Genetic control of neuronal activity in mice conditionally expressing TRPV1. Nat. Methods. 2008; 5:299–302. [PubMed: 18327266]
14. Parekh AB, Penner R. Store depletion and calcium influx. Physiol. Rev. 1997; 77:901–930. [PubMed: 9354808]
15. Smith GD, et al. TRPV3 is a temperature-sensitive vanilloid receptor-like protein. Nature. 2002; 418:186–190. [PubMed: 12077606]
16. Valenzano KJ, et al. N-(4-tertiarybutylphenyl)-4-(3-chloropyridin-2-yl)tetrahydropyrazine -1(2H)-carbox-amide (BCTC), a novel, orally effective vanilloid receptor 1 antagonist with analgesic properties: I. in vitro characterization and pharmacokinetic properties. J. Pharmacol. Exp. Ther. 2003; 306:377–386. [PubMed: 12721338]
17. Wahl P, Foged C, Tullin S, Thomsen C. Iodo-resiniferatoxin, a new potent vanilloid receptor antagonist. Mol. Pharmacol. 2001; 59:9–15. [PubMed: 11125018]
18. Barr VA, Bernot KM, Shaffer MH, Burkhardt JK, Samelson LE. Formation of STIM and Orai complexes: puncta and distal caps. Immunol. Rev. 2009; 231:148–159. [PubMed: 19754895]
19. Oh-hora M. Calcium signaling in the development and function of T-lineage cells. Immunol. Rev. 2009; 231:210–224. [PubMed: 19754899]
20. Hanke JH, et al. Discovery of a novel, potent, and Src family-selective tyrosine kinase inhibitor. Study of Lck- and FynT-dependent T cell activation. J. Biol. Chem. 1996; 271:695–701. [PubMed: 8557675]
21. Jin X, et al. Modulation of TRPV1 by nonreceptor tyrosine kinase, c-Src kinase. Am. J. Physiol. Cell. Physiol. 2004; 287:C558–63. [PubMed: 15084474]
22. Yao X, Kwan HY, Huang Y. Regulation of TRP channels by phosphorylation. Neurosignals. 2005; 14:273–280. [PubMed: 16772730]
23. Zhang X, Huang J, McNaughton PA. NGF rapidly increases membrane expression of TRPV1 heat-gated ion channels. EMBO J. 2005; 24:4211–4223. [PubMed: 16319926]
24. Straus DB, Weiss A. Genetic evidence for the involvement of the lck tyrosine kinase in signal transduction through the T cell antigen receptor. Cell. 1992; 70:585–593. [PubMed: 1505025]
25. Wirtz S, Neurath MF. Mouse models of inflammatory bowel disease. Adv. Drug Deliv. Rev. 2007; 59:1073–1083. [PubMed: 17825455]
26. Berg DJ, et al. Rapid development of colitis in NSAID-treated IL-10-deficient mice. Gastroenterology. 2002; 123:1527–1542. [PubMed: 12404228]
27. Launay P, et al. TRPM4 regulates calcium oscillations after T cell activation. Science. 2004; 306:1374–1377. [PubMed: 15550671]
28. Philipp S, et al. TRPC3 mediates T cell receptor-dependent calcium entry in human T-lymphocytes. J. Biol. Chem. 2003; 278:26629–26638. [PubMed: 12736256]
29. Caterina MJ, et al. Impaired nociception and pain sensation in mice lacking the capsaicin receptor. Science. 2000; 288:306–313. [PubMed: 10764638]
30. Schumacher MA, Moff I, Sudanagunta SP, Levine JD. Molecular cloning of an N-terminal splice variant of the capsaicin receptor. Loss of N-terminal domain suggests functional divergence among capsaicin receptor subtypes. J. Biol. Chem. 2000; 275:2756–2762. [PubMed: 10644739]
31. Saunders CI, Kunde DA, Crawford A, Geraghty DP. Expression of transient receptor potential vanilloid 1 (TRPV1) and 2 (TRPV2) in human peripheral blood. Mol. Immunol. 2007; 44:1429–1435. [PubMed: 16777226]

32. Engler A, et al. Expression of transient receptor potential vanilloid 1 (TRPV1) in synovial fibroblasts from patients with osteoarthritis and rheumatoid arthritis. Biochem. Biophys. Res. Commun. 2007; 359:884–888. [PubMed: 17560936]
33. Spinsanti G, et al. Quantitative Real-Time PCR detection of TRPV1-4 gene expression in human leukocytes from healthy and hyposensitive subjects. Mol. Pain. 2008; 4:51–8069-4-51. [PubMed: 18983665]
34. Bachiocco V, et al. Lymphocyte TRPV 1-4 gene expression and MIF blood levels in a young girl clinically diagnosed with HSAN IV. Clin. J. Pain. 2011; 27:631–634. [PubMed: 21436684]
35. Shin JS, et al. Differences in sensitivity of vanilloid receptor 1 transfected to human embryonic kidney cells and capsaicin-activated channels in cultured rat dorsal root ganglion neurons to capsaicin receptor agonists. Neurosci. Lett. 2001; 299:135–139. [PubMed: 11166956]
36. Voolstra O, Huber A. Post-Translational Modifications of TRP Channels. Cells. 2014; 3:258–287. [PubMed: 24717323]
37. Armstrong DL, Erxleben C, White JA. Patch clamp methods for studying calcium channels. Methods Cell Biol. 2010; 99:183–197. [PubMed: 21035687]
38. Gad M, Pedersen AE, Kristensen NN, Fernandez Cde F, Claesson MH. Blockage of the neurokinin 1 receptor and capsaicin-induced ablation of the enteric afferent nerves protect SCID mice against T cell-induced chronic colitis. Inflamm. Bowel Dis. 2009; 15:1174–1182. [PubMed: 19326358]
39. Moran MM, McAlexander MA, Biro T, Szallasi A. Transient receptor potential channels as therapeutic targets. Nat. Rev. Drug Discov. 2011; 10:601–620. [PubMed: 21804597]
40. Kedei N, et al. Analysis of the native quaternary structure of vanilloid receptor 1. J. Biol. Chem. 2001; 276:28613–28619. [PubMed: 11358970]

REFERENCES (Methods)

41. Moqrich A, et al. Impaired thermosensation in mice lacking TRPV3, a heat and camphor sensor in the skin. Science. 2005; 307:1468–1472. [PubMed: 15746429]
42. Gonzalez-Navajas JM, et al. Interleukin 1 receptor signaling regulates DUBA expression and facilitates Toll-like receptor 9-driven antiinflammatory cytokine production. J. Exp. Med. 2010; 207:2799–2807. [PubMed: 21115691]
43. Franco A, Shimizu C, Tremoulet AH, Burns JC. Memory T cells and characterization of peripheral T cell clones in acute Kawasaki disease. Autoimmunity. 2010; 43:317–324. [PubMed: 20166878]
44. Srikanth S, Jung HJ, Ribalet B, Gwack Y. The intracellular loop of Orai1 plays a central role in fast inactivation of Ca2+ release-activated Ca2+ channels. J. Biol. Chem. 2010; 285:5066–5075. [PubMed: 20007711]
45. Fu G, Gascoigne NR. Multiplexed labeling of samples with cell tracking dyes facilitates rapid and accurate internally controlled calcium flux measurement by flow cytometry. J. Immunol. Methods. 2009; 350:194–199. [PubMed: 19647745]
46. Fu G, et al. Themis controls thymocyte selection through regulation of T cell antigen receptormediated signaling. Nat. Immunol. 2009; 10:848–856. [PubMed: 19597499]
47. Gonzalez-Navajas JM, et al. TLR4 signaling in effector CD4+ T cells regulates TCR activation and experimental colitis in mice. J. Clin. Invest. 2010; 120:570–581. [PubMed: 20051628]
48. Li X, et al. Divergent requirement for Galphas and cAMP in the differentiation and inflammatory profile of distinct mouse Th subsets. J. Clin. Invest. 2012; 122:963–973. [PubMed: 22326954]

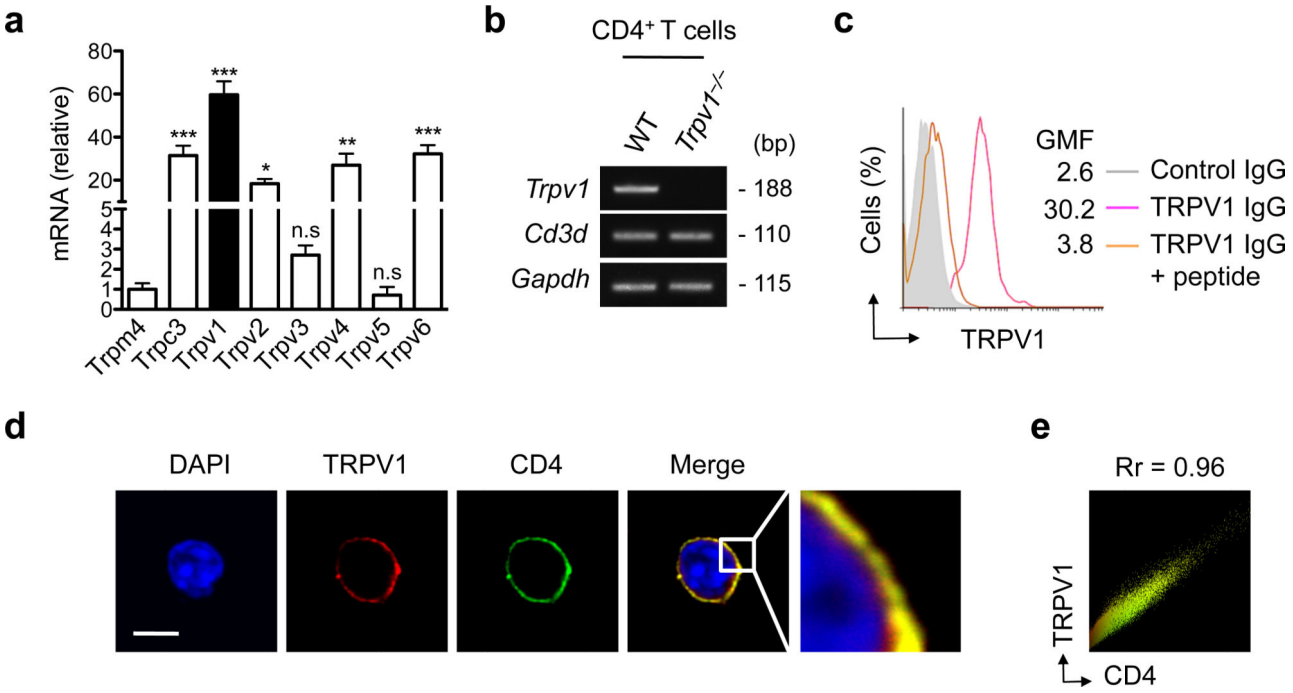

Figure 1.

TRPV1 is expressed in CD4$^+$ T cells. **(a)** Splenic (SP) CD4$^+$ T cells were isolated from C57BL/6 mice (i.e., WT) and expression of several *Trp* channels was analyzed by qPCR. Expression of *Trp* transcripts was normalized to *Gapdh* housekeeping gene and expressed relative to *Trpm4* (known to be expressed in CD4$^+$ T cells[27]). Mean ± SEM of 5 mice are shown. n.s: not significant; **P* <0.05; ****P* <0.001; *****P* <0.0001 (one-way ANOVA with post hoc Dunnett's test). **(b)** SP CD4$^+$ T cells were isolated from WT and *Trpv1*$^{-/-}$ mice and FACS-sorted CD4$^+$TCRβ$^+$ T cells (purity > 98%) were used to analyze TRPV1 expression by qPCR. PCR products from the qPCR reaction were separated on a 2% agarose gel. *Trpv1*-specific PCR product was detected with an expected size of 188 bp. *Cd3d* was used as a T cell marker and *Gapdh* as a loading control. **(c)** Splenocytes were isolated from WT mice, stained for CD4, TCRβ and TRPV1 and analyzed by flow cytometry. The histogram of TRPV1 expression on gated CD4$^+$TCRβ$^+$ T cells is shown (red line peak). The specificity of the TRPV1 Ab was confirmed by pre-incubating it with the corresponding blocking peptide (orange line peak). IgG control (grey peak). Geometric Mean Fluorescence (GMF) intensity is indicated. **(d)** Confocal images showing TRPV1 and CD4 subcellular localization in SP CD4$^+$ T cells. DAPI (left panel), TRPV1-AF546 (mid-left panel), CD4-AF488 (mid-right panel) and the merge (right panel) are shown. Scale bar = 5 μm. Yellow color in the merge panel indicates high TRPV1 and CD4 colocalization. **(e)** TRPV1 and CD4 colocalization scatter plot was generated using Velocity®. Data are representative of three or more independent experiments.

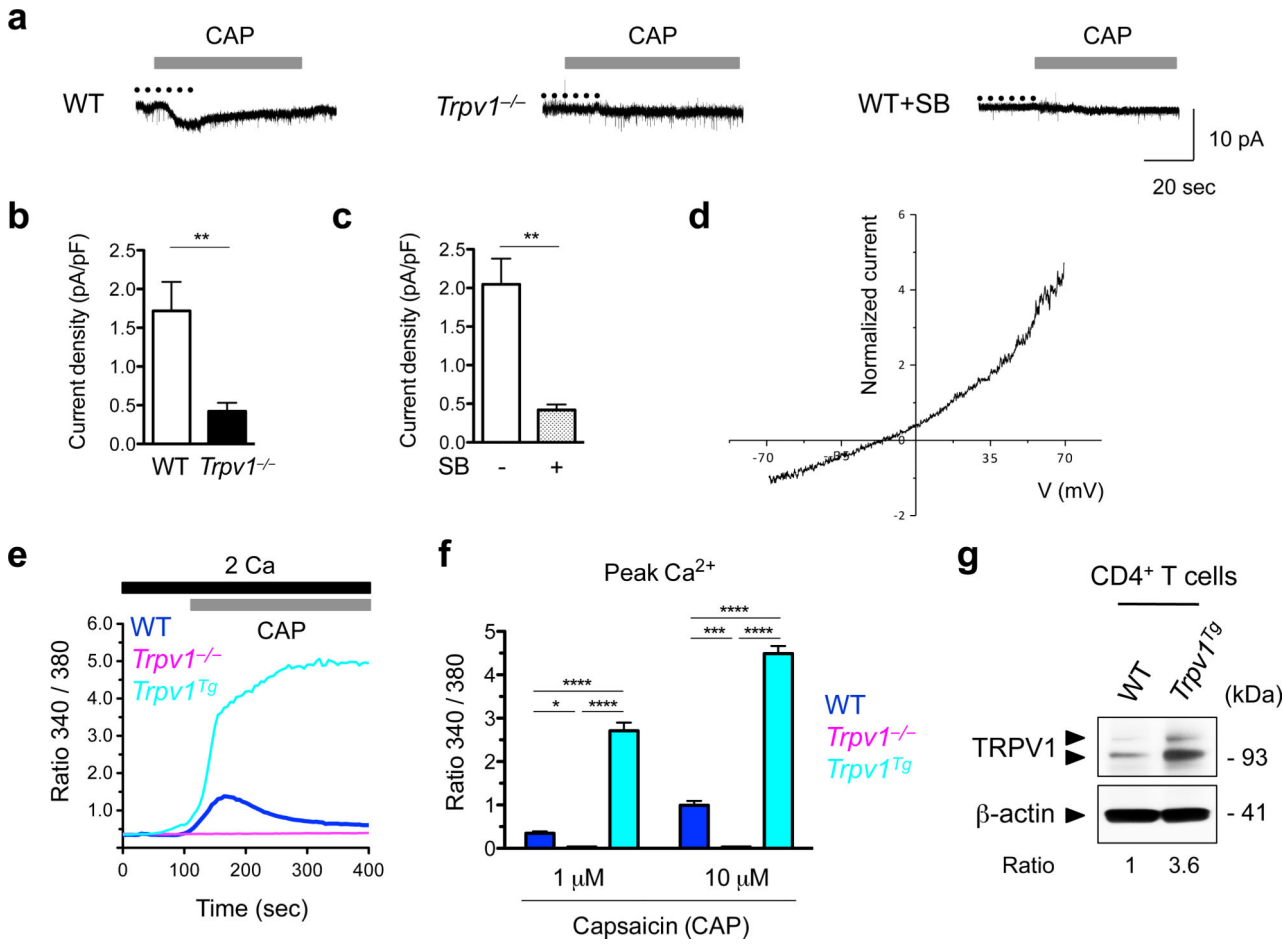

Figure 2.

TRPV1 is a functional in Ca^{2+} channel in $CD4^+$ T cells. **(a)** Sample traces of inward currents recorded on WT, *Trpv1*$^{-/-}$ and SB366791 (SB)-treated WT $CD4^+$ T cells following application of the prototypical TRPV1 agonist, capsaicin (CAP, 16 μM). Cells were held at −85 mV. Horizontal bars denote the duration of the CAP exposure. Dotted lines indicate the zero current level. **(b)** Current density comparison between WT (n = 9) and *Trpv1*$^{-/-}$ (n = 8) $CD4^+$ T cells following CAP application. Values were obtained by normalizing peak current recorded at −85 mV to capacitance of each cell. Error bars represent mean ± SEM. ***P* <0.01 (two-tailed Student t-test). **(c)** Current density comparison between untreated (n = 10) and SB-treated (1 μM; n = 13) WT $CD4^+$ T cells in response to CAP. Error bars represent mean ± SEM. *****p* <0.0001 (two-tailed Student t-test). **(d)** Current-voltage relationship (I-V curve) of CAP-evoked current in $CD4^+$ T cells exhibits outward rectification. A voltage ramp was delivered from −70 mV to +70 mV in 400-ms. CAP-evoked current was isolated by subtracting current before and after addition of CAP (3 μM). Currents were normalized relative to the current at −70 mV (−19.2±3.3 pA) and data is presented as the average of I-V curves from n = 4 cells. **(e)** WT (blue line), *Trpv1*$^{-/-}$ (magenta line) and *Trpv1*^{Tg} (turquoise line) SP $CD4^+CD25^-$(naive) T cells were isolated, loaded with Fura-2 AM and changes in $[Ca^{2+}]_i$ following application of CAP (10 μM) in the presence of 2 mM $CaCl_2$ (2 Ca) were monitored by confocal imaging. **(f)** Statistical analysis of the Ca^{2+} influx profiles shown in **e**

for CAP (1 or 10 μM). Mean ± SEM of 50-100 individual cells. *P <0.05; ***P <0.001; ****P <0.0001 (one-way ANOVA with post hoc Bonferroni test). **(g)** SP $CD4^+$ T cells were isolated from WT and *Trpv1*^{Tg} mice and TRPV1 expression in total cell lysates was analyzed by immunoblotting. Immunoreactive doublets at ≈ 95 and 115 kDa correspond to the non-glycosylated and glycosylated forms of the TRPV1 channel[40]. Data are representative of three or more independent experiments.

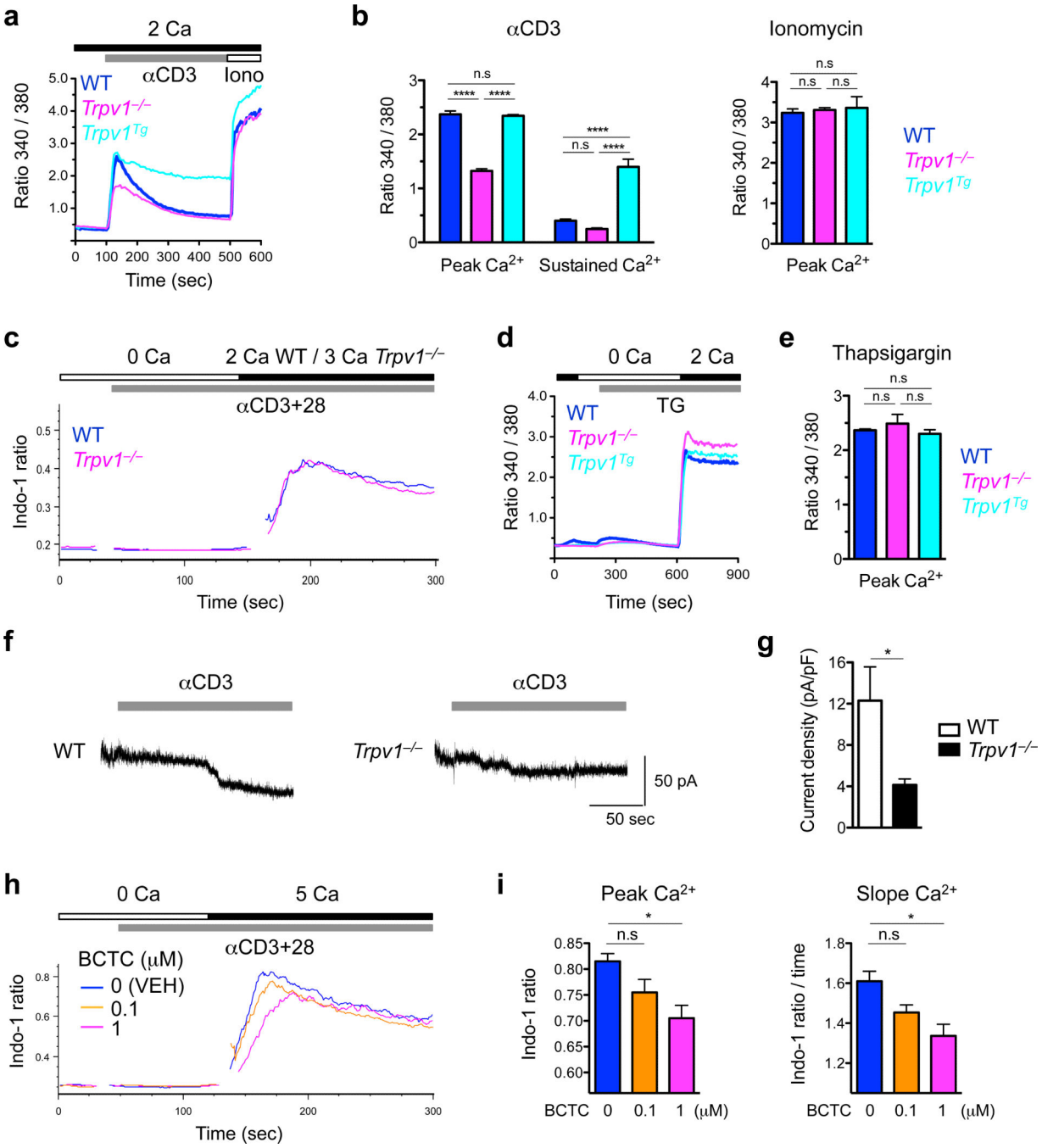

Figure 3.

TRPV1^{CD4} acts as a non-store-operated Ca^{2+} channel and contributes to TCR-induced Ca^{2+} influx. WT (blue line), *Trpv1*$^{-/-}$ (magenta line) and *Trpv1*^{Tg} (turquoise line) SP $CD4^+CD25^-$ (naive) T cells were isolated, loaded with Fura-2 AM and changes in $[Ca^{2+}]_i$ were monitored by confocal imaging. **(a)** Cells were stimulated by anti-CD3 crosslinking in the presence of 2 mM $CaCl_2$ (2 Ca) and ionomycin (Iono, 1 μM) was added at the end of the acquisition. **(b)** Statistical analysis of the Ca^{2+} influx profiles shown in **a**. Mean ± SEM of 50-100 individual cells. **(c)** WT and *Trpv1*$^{-/-}$ SP $CD4^+$ T cells were isolated, loaded with

Indo-1 AM and stimulated with soluble anti-CD3 (10 μg/mL) and anti-CD28 (1 μg/mL) in Ca^{2+}-free medium. Changes in $[Ca^{2+}]_i$ were monitored by flow cytometry and overlay of the Ca^{2+} influx profiles after addition of $CaCl_2$ (2 mM/WT, 3 mM/*Trpv1*$^{-/-}$) to the extracellular medium is shown. **(d)** Store-operated Ca^{2+} measurements were performed after passive depletion of intracellular stores using 1 μM thapsigargin (TG). **(e)** Statistical analysis of the Ca^{2+} influx profiles shown in **d**. Mean ± SEM of 50-100 individual cells is shown. **(f)** Sample traces of inward currents in WT and *Trpv1*$^{-/-}$ $CD4^+$ T cells activated by anti-CD3 crosslinking and held at −85mV. Bar donates the duration of streptavidin application. **(g)** Comparison of TCR-induced currents in WT (n = 7) and *Trpv1*$^{-/-}$ (n = 9) $CD4^+$ T cells. Values were obtained by normalizing peak current to capacitance of each cell. **(h)** WT $CD4^+$ T cells were pretreated with the indicated concentrations of a specific TRPV1 antagonist (BCTC) or the vehicle (VEH; 0.1% DMSO) for 5 min. Cells were then stimulated with anti-CD3+28 in Ca^{2+}-free medium and $CaCl_2$ (5 mM) was added to the extracellular medium during the acquisition. **(i)** Statistical analysis of the Ca^{2+} influx profiles shown in **f.** Mean ± SEM of thrndent experiments is shown. n.s: not significant; **P* <0.05; ***P* <0.01; *****p* <0.0001 (two-tailed Student t-test [**g**], one-way ANOVA with post hoc Bonferroni test [**b,e,i**]). Data are representative of three or more independent experiments.

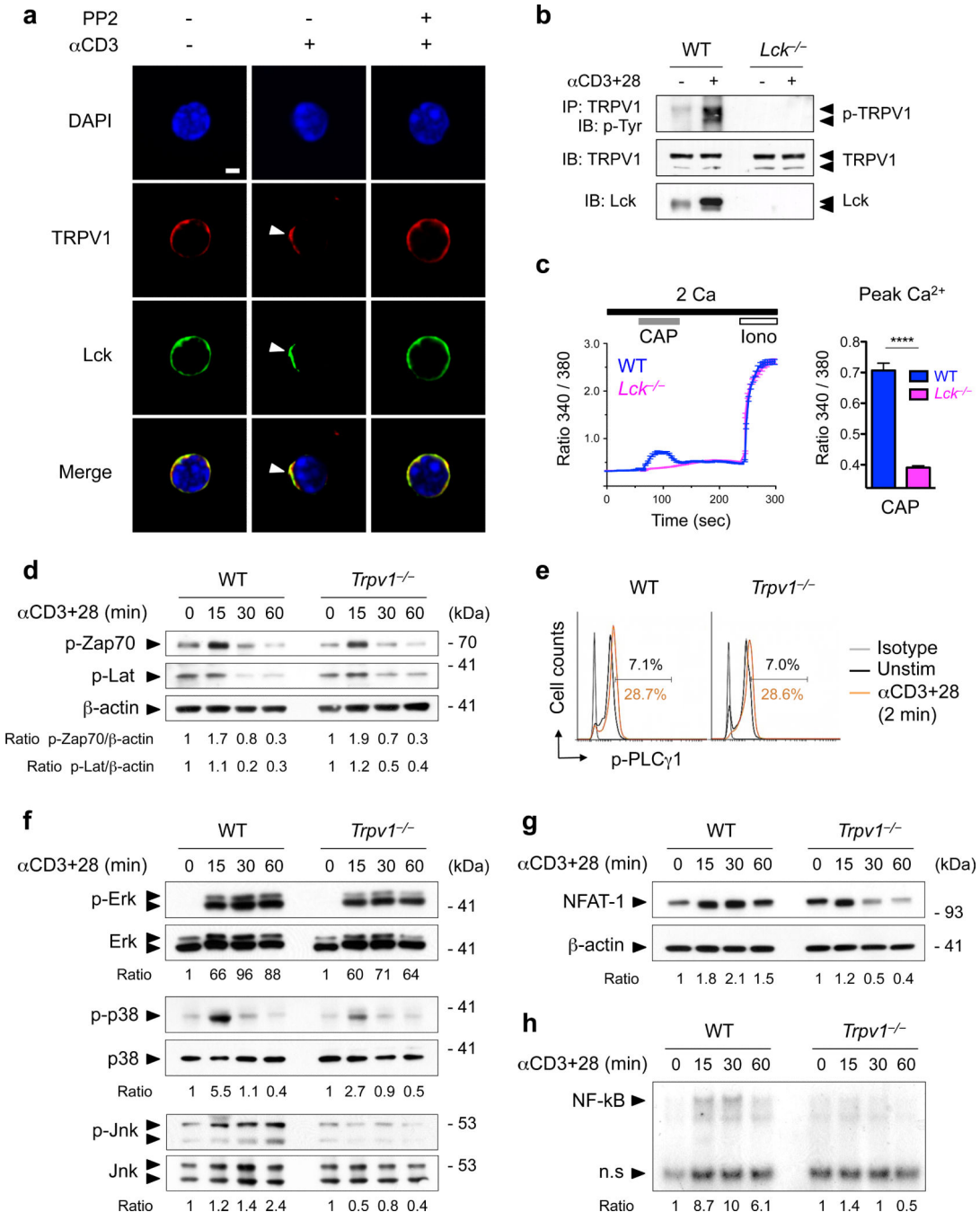

Figure 4.

TRPV1^{CD4} participates in TCR signaling. **(a)** Confocal images of Lck and TRPV1 clustering induced by anti-CD3 crosslinking. TRPV1 and Lck fluorescence signals largely colocalized in resting WT SP CD4^{+} T cells as indicated by the yellow color in the merge panel. In addition, TRPV1 is recruited to TCR clusters upon TCR liagtion (white arrowheads). The Src-family kinase inhibitor PP2 (10 μM) inhibits Lck and TRPV1 capping. Scale bar = 2 μm. **(b)** Jurkat cell clones E6.1 (WT) and J.Cam1.6 (*Lck*$^{-/-}$) were left unstimulated or stimulated with soluble anti-hCD3 (2.5 μg/mL) and anti-hCD28 (1 μg/mL)

for 5 min and anti-TRPV1 immunoprecipitates (IP) or total cell lysates were analyzed by immunoblot (IB) with anti-phospho-tyrosine (p-Tyr) or with anti-TRPV1 and anti-Lck, respectively. **(c)** WT and *Lck*$^{-/-}$ Jurkat T cells were loaded with Fura-2 AM and changes in $[Ca^{2+}]_i$ upon application of capsaicin (CAP, 1 μM) were monitored by confocal imaging. Ionomycin (Iono, 1 μM) was used as a positive control and was added at the end of the acquisition. Right panel: statistical analysis of the CAP-induced Ca^{2+} influx peak. n.s: not significant; ****P<0.0001 (two-tailed Student t-test). **(d)** WT and *Trpv1*$^{-/-}$ SP CD4$^+$ T cells were isolated and stimulated with soluble anti-CD3 (5 μg/mL) and anti-CD28 (2 μg/mL) for the indicated amount of time or left unstimulated. Phosphorylation of Zap70 and Lat was analyzed by immunoblotting in the cytosolic fraction. Densitometry analysis of the specific bands normalized to the expression of the loading control β-actin is indicated. **(e)** WT and *Trpv1*$^{-/-}$ SP CD4$^+$ T cells were isolated and stimulated with soluble anti-CD3 (5 μg/mL) and anti-CD28 (2 μg/mL) for 2 min or left unstimulated. Representative panels of phospho-PLCγ1 intracellular staining on gated CD4$^+$TCRβ$^+$ T cells are shown. **(f)** Cells were stimulated as in **d**, and phosphorylation of Erk1/2, p38 and Jnk was analyzed in the cytosolic fraction. Densitometry analysis of the specific bands normalized to the expression of the corresponding total protein is indicated. **(g)** NFAT-1 translocation in the nuclear fraction. **(h)** EMSA analysis of NF-κB translocation in the nuclear fraction. A nonspecific low molecular weight band (n.s) on the same gel was used to verify equivalent loading. Data are representative of three ore more independent experiments.

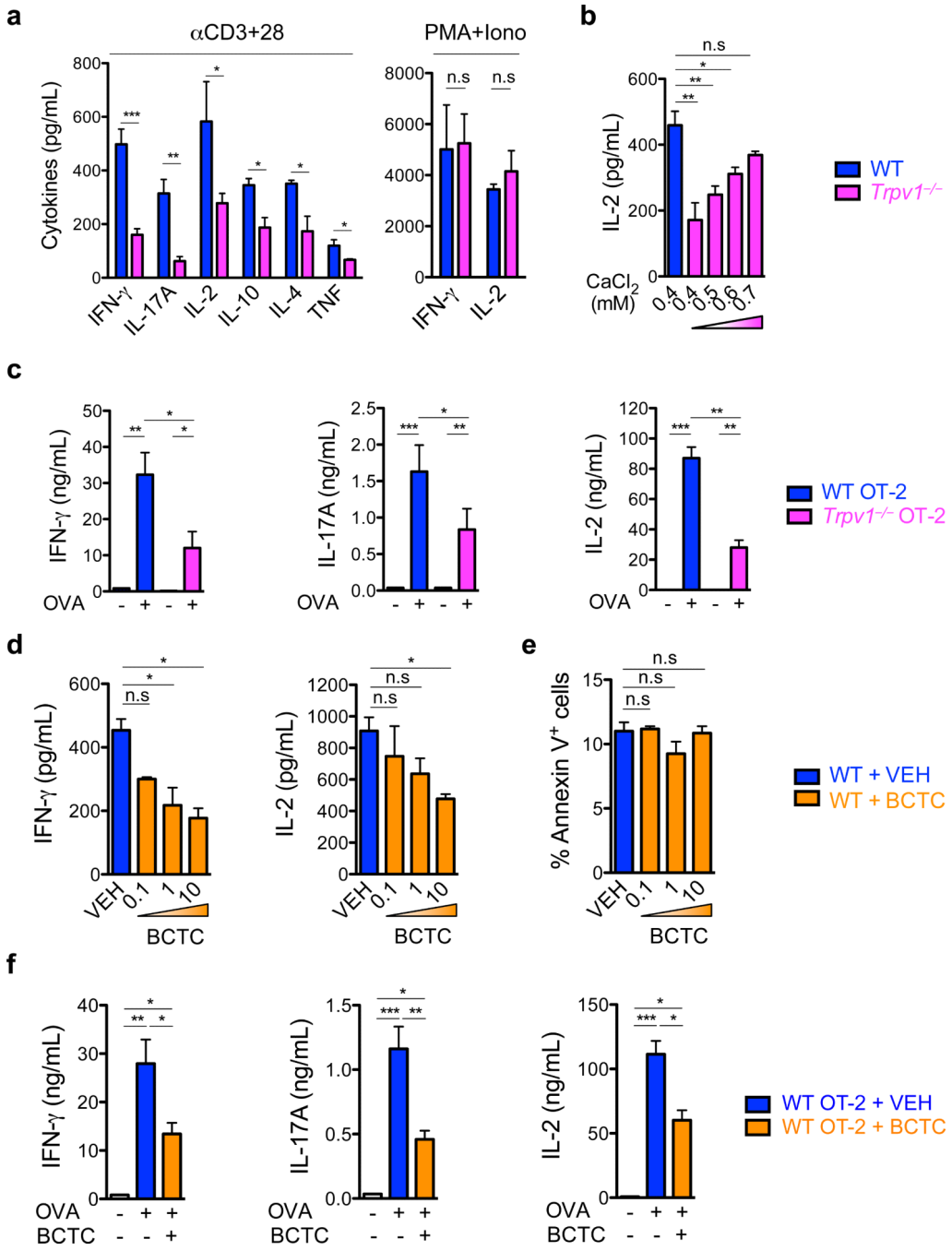

Figure 5.

Genetic deletion or pharmacological inhibition of TRPV1^{CD4} decreases TCR-induced cytokine production. Splenic CD4$^+$ T cells were isolated from WT and *Trpv1*$^{-/-}$ mice. **(a)** Cells were stimulated with anti-CD3 (10 μg/mL plate-bound) and anti-CD28 (1 μg/mL soluble) [left panel] or with PMA (25 ng/mL) and ionomycin (500 nM) [right panel] for 24 (IFN-γ, IL-17A, IL-2, TNF) or 48h (IL-10, IL-4) and cytokine production was assessed by ELISA (n = 3-6 mice/group). **(b)** WT and *Trpv1*$^{-/-}$ CD4$^+$ T cells were stimulated with anti-CD3+28 for 24h in RPMI supplemented with indicated concentrations of $CaCl_2$.

Supernatants were collected and IL-2 production was measured (n = 3 mice/group). **(c)** OVA-loaded splenic $CD11c^+$ DCs from WT mice were incubated with OVA-specific $CD4^+$ T cells isolated from the spleen of WT OT-2 or *Trpv1*$^{-/-}$ OT-2 mice. After five days of co-culture, $CD4^+$ T cells were recovered, counted and equal numbers of cells were re-stimulated with anti-CD3+28 for 24h. Supernatants were collected and IFN-γ, IL-17A and IL-2 levels were measured (n = 4 mice/group). **(d)** WT splenic $CD4^+$ T cells were pre-incubated with the indicated concentrations of BCTC (a TRPV1 inhibitor) or its vehicle (0.1% DMSO) for 30 min and stimulated with anti-CD3+28 for 24h. Supernatants were collected and IFN-γ (left-panel) and IL-2 (right-panel) production was assessed by ELISA (n = 3 mice/group). **(e)** Cells from the ELISA shown in **d** were recovered, stained for CD4, Annexin-V and 7-AAD and $CD4^+$ T cell apoptosis was analyzed by flow cytometry. **(f)** Splenic $CD4^+$ T cells from OT-2 mice were pre-treated with BCTC (1 μM) or with vehicle (0.1% DMSO) for 30 min, washed and cultured with OVA-loaded splenic DC from WT mice. After five days of co-culture, $CD4^+$ T cells were processed as described in **c** and cytokine production was assessed (n = 4 mice/group). Data are representative of five (**a**, left panel), three (**b-d, f**) or two (**a**, right panel; **e**) independent experiments.. n.s: not significant; $*P<0.05$; $**P<0.01$; $***P<0.001$; $****P<0.0001$ (two-tailed Student t-test [**a**], one-way ANOVA with post hoc Bonferroni [**c,f**] or Dunnett's [**b,d,e**] tests).

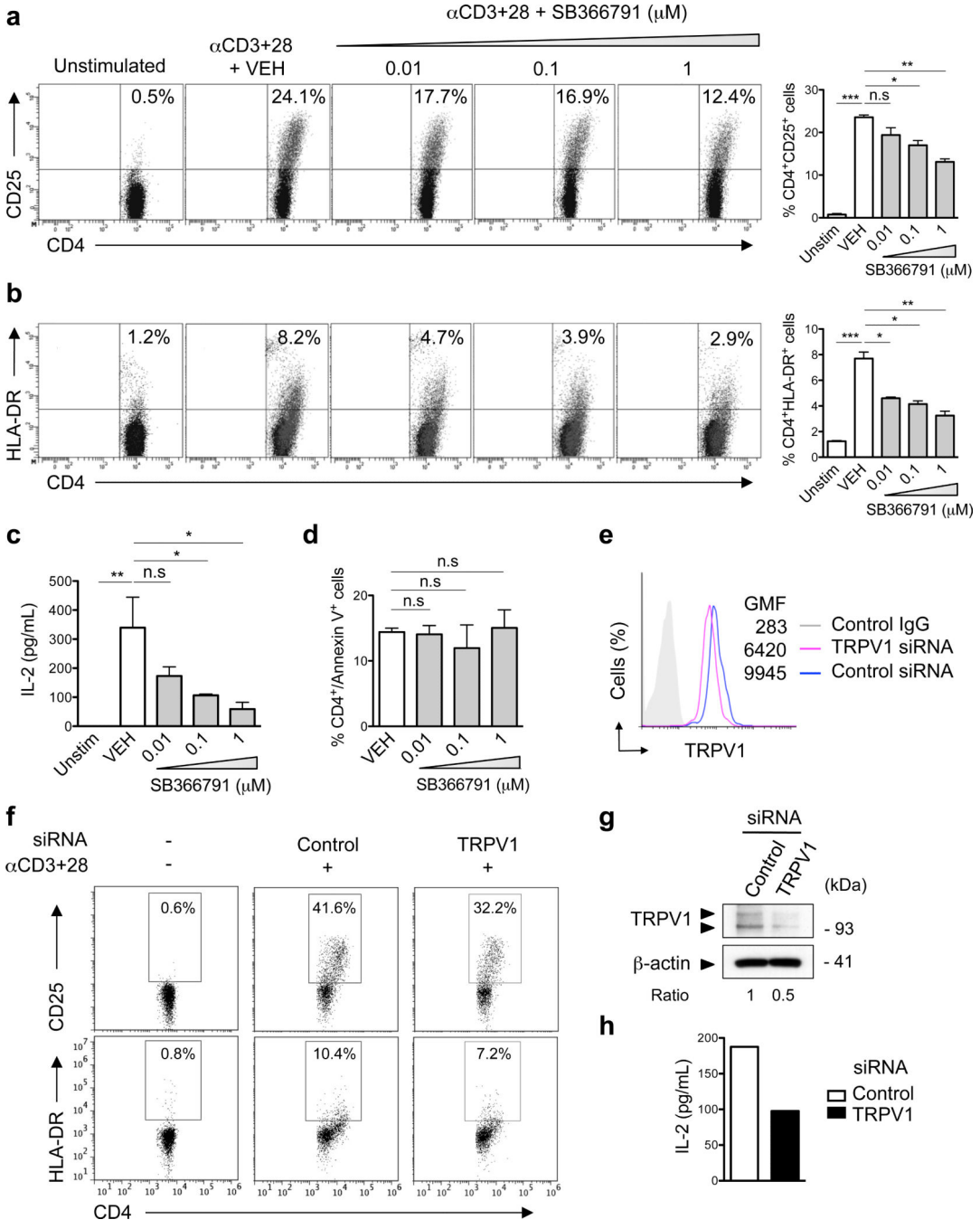

Figure 6.

Genetic and pharmacological inhibition of TRPV1^{CD4} decrease human primary CD4$^+$ T cell activation. PBMCs were isolated from healthy human donors and stimulated with anti-CD3+28 (both 1 μg/mL soluble) in the presence of indicated concentrations of a TRPV1 antagonist (SB366791) or its vehicle (0.1% DMSO) for 48h. **(a, b)** Cells were stained for CD4, CD25 and HLA-DR, and analyzed by flow cytometry. The % of CD4$^+$CD25$^+$ cells and CD4$^+$HLA-DR$^+$ cells are indicated (right panels). **(c)** The supernatants were collected and IL-2 production was measured. **(d)** Cells were stained for CD4 and Annexin-V and

$CD4^+$ T cell apoptosis was analyzed by flow cytometry. **(e)** Freshly isolated PBMCs were nucleofected with a TRPV1 siRNA or a nontargeting (control) siRNA and stimulated with anti-CD3+28 6h after transfection. TRPV1 knockdown efficiency and **(f)** expression of surface activation markers, i.e., CD25 and HLA-DR were quantified on gated $CD4^+$ T cells, 48h after transfection and 42h after anti-CD3+28 Abs stimulation, respectively. Transfection with TRPV1 siRNA reduced TRPV1 expression on gated $CD4^+$ T cells by 40%, as well as CD25 and HLA-DR upregulation by 25% and 30%, respectively. **(g)** TRPV1 knockdown efficiency in a human $CD4^+$ T cell clone was determined by immunoblot and IL-2 production was measured by ELISA **(h)** 48h after transfection and 42h after anti-CD3+28 stimulation respectively. TRPV1 expression and IL-2 production were reduced by 50% in TRPV1 knockdown $CD4^+$ T cells compared to control siRNA-transfected cells. Representative panels of 4 **(a-d)** or 3 **(e-h)** independent experiments and mean ± SEM of 2 or 3 individual healthy donors are shown. n.s: not significant; $*P<0.05$; $**P<0.01$; $***P<0.001$; $****P<0.0001$ (one-way ANOVA with post hoc Dunnett's test).

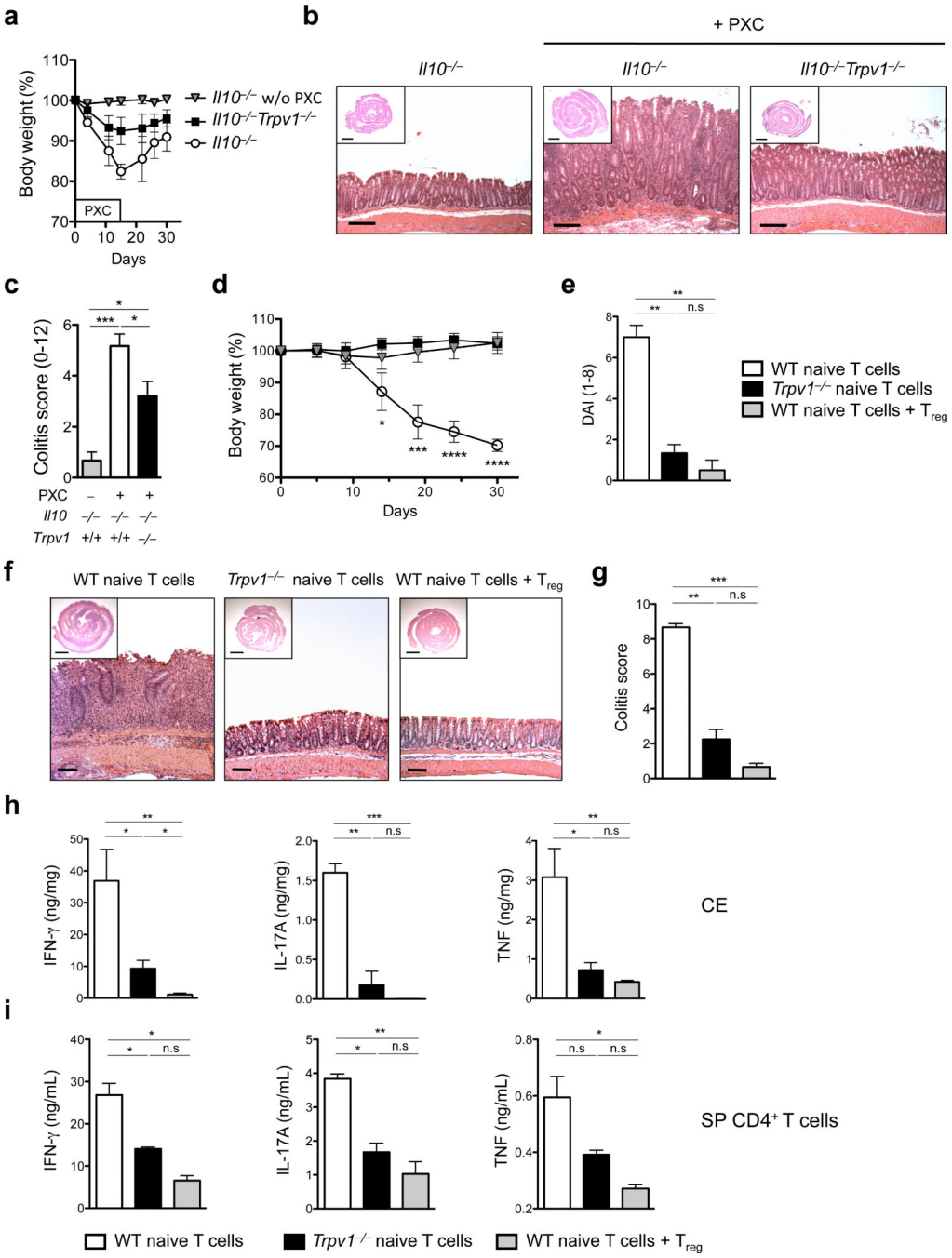

Figure 7.

TRPV1^{CD4} regulates T cell-mediated colitis. **(a)** Wasting disease in *Il10*$^{-/-}$ and *Il10*$^{-/-}$ *Trpv1*$^{-/-}$ mice after colitis induction and synchronization by Piroxicam (PXC). Statistical analysis compared *Il10*$^{-/-}$ and *Il10*$^{-/-}$ *Trpv1*$^{-/-}$ groups. **(b)** Representative pictures (1× and 20× objectives) of colon sections stained with H&E. Scale bar = 1 mm (overview insets), 100 μm (high-power fields). **(c)** Colitis score of the 3 different groups. **(d)** Percentage of initial body weight of *Rag1*$^{-/-}$ recipient mice 4 weeks post-adoptive transfer with 3×10^5 WT or *Trpv1*$^{-/-}$ flow-sorted naive (CD4$^+$CD45RB^{hi}CD25$^-$) T cells, or with

3×10^5 WT naive $CD4^+$ T cells + 1.5×10^5 WT T_{reg} cells ($CD4^+CD45RB^{lo}CD25^+$). Statistical analysis compared WT naive $CD4^+$ T cell and *Trpv1*$^{-/-}$ naive $CD4^+$ T cell groups. **(e)** Disease Activity Index (DAI) in the different groups. **(f)** Representative pictures (1× and 20× objectives) of colon sections stained with H&E. Scale bar = 1 mm (overview insets), 100 μm (high-power fields). **(g)** Colitis score of the different groups. **(h)** Cytokine concentrations in colonic explants after 24h culture. **(i)** Cytokine production by splenic $CD4^+$ T cells isolated from *Rag1*$^{-/-}$ recipients, 24h after re-stimulation with anti-CD3 (10 μg/mL plate-bound) and anti-CD28 (1 μg/mL soluble). One representative experiment out of two (*Il10*$^{-/-}$ model) or three (*Rag1*$^{-/-}$ model) is shown. Mean ± SEM (n = 6-7 **[a-c]**, 6-8 **[d-g]** or 4 **[h,i]** mice/group). n.s: not significant; *P <0.05; **P <0.01; ***P <0.001; ****P <0.0001 (one-way **[c,e,g-i]** or two-way **[a, d]** ANOVA with post hoc Bonferroni test).

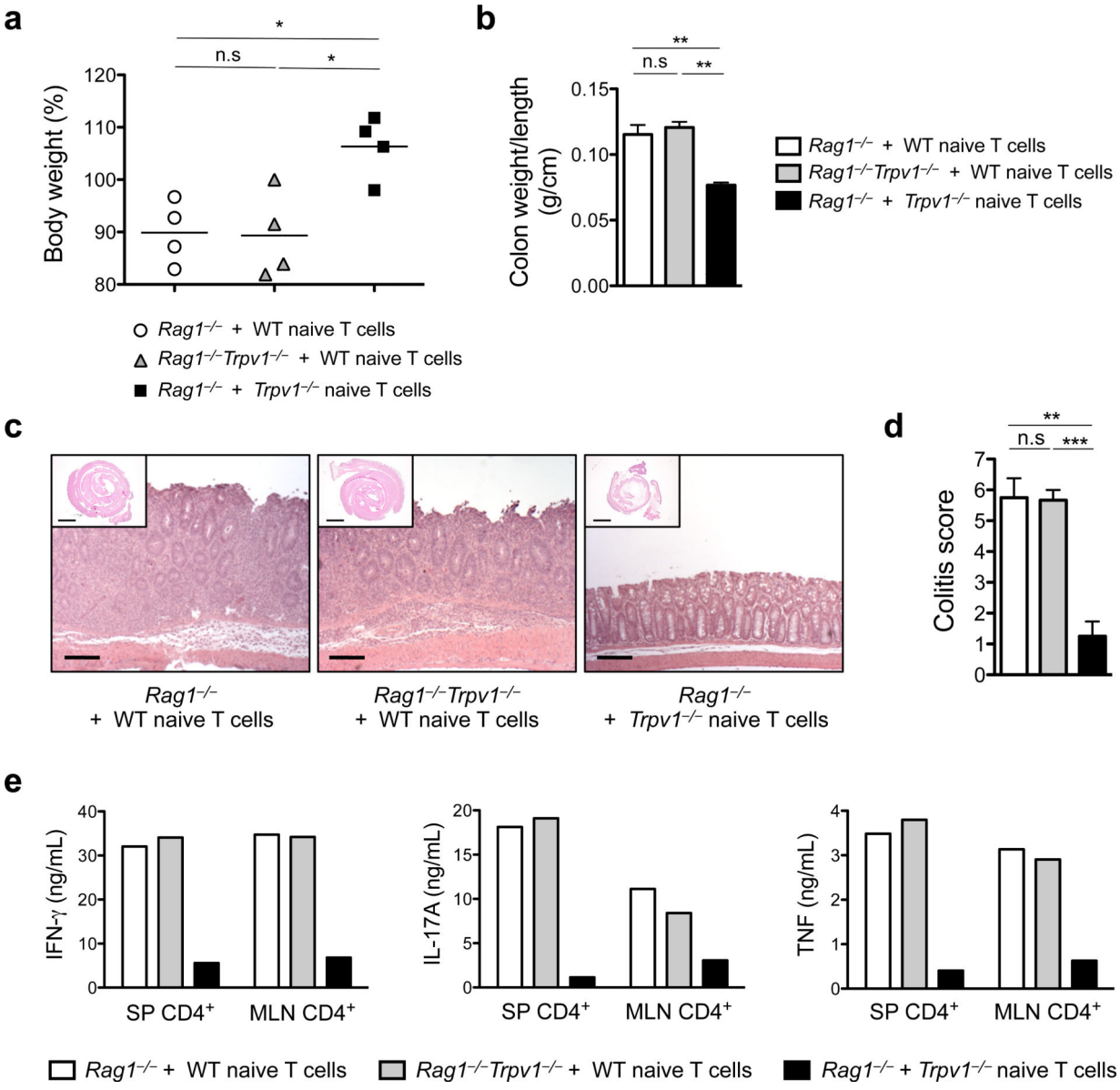

Figure 8.

TRPV1 expression in non-CD4$^+$ T cells does not affect colitis severity in an adoptive transfer model. **(a)** Wasting disease 4 weeks post-transfer. Percentage of initial body weight of *Rag1*$^{-/-}$ or *Rag1*$^{-/-}$ *Trpv1*$^{-/-}$ recipient mice transferred with 3×10^5 WT or *Trpv1*$^{-/-}$ FACS-sorted naive (CD4$^+$CD45RB^{high}CD25$^-$) T cells. **(b)** Colon weight/length ratio. **(c)** Representative pictures (1× and 20× objectives) of colon sections stained with H&E. Scale bar = 1mm (overview insets), 100 μm (high-power fields). **(d)** Colitis score. **(e)** Cytokine production by pooled SP and MLN CD4$^+$ T cells, 24h after re-stimulation with anti-CD3 (10 μg/mL plate-bound) and anti-CD28 (1 μg/mL soluble) (ELISA). Data are representative of two independent experiments. Results are expressed as mean ± SEM (n = 4 mice/group). n.s: not significant; **P* <0.05 ; ****P* <0.001 (one-way ANOVA with post hoc Bonferroni test).